Journal of Systematic Palaeontology
Publication details, including instructions for authors and subscription information:
http://www.tandfonline.com/loi/tjsp20

Biogeographical implications of a new mouse-sized fossil bandicoot (Marsupialia: Peramelemorphia) occupying a dasyurid-like ecological niche across Australia

Yamila Gurovich [a b], Kenny J. Travouillon [a c], Robin M. D. Beck [a d], Jeanette Muirhead [a] & Michael Archer [a]

[a] School of Biological, Earth and Environmental Sciences, University of New South Wales, New South Wales, 2052, Australia

[b] CONICET and Laboratorio de Investigaciones en Evolución y Biodiversidad, Universidad Nacional de la Patagonia, Sarmiento 849, Esquel, Chubut, 9200, Argentina

[c] School of Earth Sciences, University of Queensland, St Lucia, Queensland, 4072, Australia

[d] Department of Mammalogy, American Museum of Natural History, Central Park West at 79th Street, New York, NY, 10024, USA

Published online: 22 May 2013.

To cite this article: Yamila Gurovich, Kenny J. Travouillon, Robin M. D. Beck, Jeanette Muirhead & Michael Archer (2013): Biogeographical implications of a new mouse-sized fossil bandicoot (Marsupialia: Peramelemorphia) occupying a dasyurid-like ecological niche across Australia, Journal of Systematic Palaeontology, DOI:10.1080/14772019.2013.776646

To link to this article: http://dx.doi.org/10.1080/14772019.2013.776646

Journal of Systematic Palaeontology, 2013
http://dx.doi.org/10.1080/14772019.2013.776646

Biogeographical implications of a new mouse-sized fossil bandicoot (Marsupialia: Peramelemorphia) occupying a dasyurid-like ecological niche across Australia

Yamila Gurovich[a,b*], Kenny J. Travouillon[a,c], Robin M. D. Beck[a,d], Jeanette Muirhead[a] and Michael Archer[a]

[a]*School of Biological, Earth and Environmental Sciences, University of New South Wales, New South Wales 2052, Australia;* [b]*CONICET and Laboratorio de Investigaciones en Evolución y Biodiversidad, Universidad Nacional de la Patagonia, Sarmiento 849, Esquel, Chubut 9200, Argentina;* [c]*School of Earth Sciences, University of Queensland, St Lucia, Queensland 4072, Australia;* [d]*Department of Mammalogy, American Museum of Natural History, Central Park West at 79th Street, New York, NY 10024, USA*

(Received 18 January 2012; accepted 10 July 2012)

We describe *Bulungu palara* gen. et sp. nov., a new fossil peramelemorphian (bandicoot), based on a single well-preserved skull and additional dental specimens from Late Oligocene to Middle Miocene (Faunal Zones A–C) limestone deposits at the Riversleigh World Heritage Property, Queensland, and two dental specimens from the Early–Middle Miocene Kutjamarpu Local Fauna, South Australia. This is the first fossil peramelemorphian species to be reported from more than a single fossil fauna, with its inferred distribution extending from north-western Queensland (modern latitude ~19°S) to north-eastern South Australia (modern latitude ~28°S). The presence of *Bulungu palara* in Riversleigh Faunal Zones A, B and C and in the Kutjamarpu Local Fauna supports the current interpretation that these faunas span similar ages, namely Late Oligocene–Middle Miocene. Phylogenetic analyses of an expanded 74 morphological character dataset using maximum parsimony and Bayesian approaches, both with and without a molecular scaffold, consistently place *Bulungu* and the Oligo-Miocene forms *Galadi* and *Yarala* outside crown-group Peramelemorphia. These analyses also fail to support a close relationship between the Pliocene *Ischnodon australis* (previously considered the oldest known representative of the extant peramelemorphian family Thylacomyidae) and the modern thylacomyid genus *Macrotis*. With an estimated body mass of ~130 g, *Bulungu palara* is smaller than any known Recent bandicoot from Australia, although some modern New Guinean species are similar in size. The small size and craniodental morphology of *B. palara* suggest that it was predominantly or exclusively insectivorous, perhaps ecologically similar to small New Guinean dasyurids such as *Murexechinus melanurus.* Together with the small-bodied (< 100 g), insectivorous *Yarala burchfieldi* and large-bodied (~900 g), faunivorous *Galadi speciosus*, *Bulungu palara* demonstrates that Oligo-Miocene Australian peramelemorphians filled ecological niches that today are mostly occupied by dasyurids, and that a major faunal turnover event occurred at some point after the Middle Miocene.

http://zoobank.org/urn:lsid:zoobank.org:pub:18955DCC-DB8C-4216-AF38-921E1E5C1F79

Keywords: *Bulungu palara*; Kutjamarpu; Miocene; morphology; phylogeny; Riversleigh

Introduction

Prior to 2000, the known fossil record of the Australasian marsupial order Peramelemorphia (which includes the > 20 Recent species of bandicoots and bilbies) comprised solely isolated teeth and jaw fragments. However, intensive collecting from Oligo-Miocene freshwater limestone deposits at Riversleigh, north-western Queensland has resulted in the discovery of numerous remarkably well-preserved fossils of multiple peramelemorphian genera, including whole skulls and associated postcranial material. These fossil peramelemorphians are providing significant new insights into the evolutionary history of this major marsupial clade.

To date, two fossil peramelemorphians have been described from Oligo-Miocene sites at Riversleigh, with both represented by relatively complete craniodental specimens: *Yarala burchfieldi* Muirhead & Filan, 1995 and *Galadi speciosus* Travouillon *et al.*, 2010. Phylogenetic analyses indicate that both *Yarala* and *Galadi* lie outside crown-group Peramelemorphia, and so they provide key information regarding the pattern of character evolution within this clade. In addition, based on their craniodental morphology, both taxa appear to have filled faunivorous ecological niches that today are largely occupied by members of another marsupial clade, namely Dasyuridae (which includes marsupial 'mice' and quolls).

Peramelemorphians are a common component of Australian fossil mammal faunas from the Late Oligocene onwards (e.g. Stirton 1955; Archer & Wade 1976; Campbell 1976; Woodburne *et al.* 1993; Muirhead & Filan 1995; Muirhead & Godthelp 1996; Muirhead *et al.* 1997;

*Corresponding author. Email: yamilag@gmail.com

Muirhead 1994, 1999, 2000; Mackness *et al.* 2000; Case 2001; Price 2002, 2005; Turnbull *et al.* 2003; Hocknull 2005; Archer *et al.* 2006; Schwartz 2006; Travouillon *et al.* 2010). As a result, they represent a very promising tool for biocorrelation of different Australian fossil sites, many of which have yet to be securely dated. However, both the phylogeny and species-level taxonomy of fossil peramelemorphians remain unclear, and hence they remain an unexploited resource for biocorrelative purposes.

Here we describe a third fossil peramelemorphian from Riversleigh, *Bulungu palara*, based on a single well-preserved skull and multiple isolated maxillae and dentaries from Riversleigh Faunal Zones A, B and C (currently interpreted as spanning the Late Oligocene to the Middle Miocene; Travouillon *et al.* 2006, 2011). In addition, we refer a right M2 and a left dentary preserving m2–3 from the Kutjamarpu Local Fauna in South Australia to *B. palara*, which is therefore the first fossil bandicoot known to occur at more than one Australian fossil locality. We assess the phylogenetic relationships of this taxon using a new morphological dataset expanded from that of Travouillon *et al.* (2010), and also discuss its ecological and biochronological implications.

Material and methods

Collecting and processing

Specimens described here from the Riversleigh World Heritage Site in Queensland have been collected over the last 30 years by researchers at the University of New South Wales. Specimens from Leaf Locality, Kutjamarpu Local Fauna (LF), South Australia were collected in 1971 by a combined South Australian Museum and University of California expedition. The Riversleigh specimens were processed in the laboratory at the University of New South Wales using an acetic acid solution of approximately 5 to 10% to dissolve the surrounding limestone that encapsulates the bones and teeth of the specimens (Archer *et al.* 1991), while the Leaf Locality specimens were obtained by screen washing in the field (Campbell 1976).

Anatomical terminology and classification

Dental terminology follows Archer (1976) and Muirhead & Filan (1995), with the homology of molar loci following Luckett (1993). Cranial anatomy follows Muirhead (1994, 2000), Wible (2003), Voss & Jansa (2003) and Beck *et al.* (2008a), unless otherwise stated. Peramelemorphian systematics follow Muirhead (1994, 2000), Muirhead & Filan (1995) and Wilson & Reeder (2005). Higher level marsupial systematics follow the classification of Aplin & Archer (1987).

Institutional abbreviations

All specimens are registered in the fossil vertebrate collection of the Queensland Museum (prefix **QM F**). **QM F** refers to Queensland Museum Fossil, **SAM P** South Australian Museum, Palaeontology Collection, South Australia. Biostratigraphica1 nomenclature follows Travouillon *et al.* (2006) and Arena (2004).

Phylogenetic analysis

To assess the phylogenetic affinities of *Bulungu palara*, we expanded the 51 craniodental character dataset of Travouillon *et al.* (2010) by adding an additional 22 characters (11 dental, 11 cranial), largely taken from Voss & Jansa (2009) and Aplin *et al.* (2010). In addition, character 15 from Travouillon *et al.* (2010) has been subdivided into two characters: morphology of the centrocrista of M1 and M2 (character 15), and morphology of the centrocrista of M3 (character 16), and both have been modified to include an extra state. As a result, the final matrix comprises 74 craniodental characters. As in Travouillon *et al.* (2010), all characters representing plausible morphoclines were ordered; 30 characters were ordered in the expanded matrix presented here (see Online Supplementary Material Appendix A); the matrix is also available for download from morphobank.org, project number 758.

We also expanded the taxon sampling of Travouillon *et al.* (2010). We added *Bulungu palara* and another fossil peramelemorphian, *Ischnodon australis* from the Pliocene Palankarinna LF; the latter has been suggested to be a plesiomorphic member of the family Thylacomyidae (see Stirton 1955), which includes the extant greater bilby *Macrotis lagotis* and the recently extinct lesser bilby *M. leucura*. We also included a denser sampling of Recent peramelemorphians by adding *Peroryctes broadbenti*, *Microperoryctes ornata*, *M. papuensis* and *Echymipera davidi* to the matrix. We retain the same outgroups used in Travouillon *et al.* (2010), namely the stem-australidelphian *Djarthia murgonensis* and the fossil dasyuromorphians *Barinya wangala* and *Mutpuracinus archibaldi*. As a result, the final matrix comprises three outgroups and 25 ingroup taxa, including 20 of the 23 currently recognized Recent peramelemorphian species (*Echymipera echinista*, *Microperoryctes aplini* and *M. murina* have not been included as we were unable to examine relevant specimens of these rare species).

Unconstrained maximum parsimony analysis of the matrix was carried out using PAUP* 4.0b10, following the two-stage strategy of Worthy *et al.* (2006) and Beck *et al.* (2008b). This comprised an initial heuristic search of 1000 random addition replicates, saving 10 trees per replicate, followed by a second heuristic search within the set of the trees saved from the first stage. A strict consensus of all most parsimonious trees was made. Decay indices (Bremer 1988) for each node in the strict consensus were calculated using the same search strategy, and bootstrap values were calculated using 250 replicates (each bootstrap replicate itself comprised 10 random addition sequence replicates).

Following Travouillon *et al.* (2010), the maximum parsimony analysis was repeated using a molecular scaffold. We

used the recent molecular phylogeny of Westerman *et al.* (2012) as a 'backbone' constraint in the molecular scaffold analysis; only those clades that received ≥70% partitioned maximum likelihood bootstrap support and ≥0.95 partitioned Bayesian posterior probability in the analyses of Westerman *et al.* (2012, table 2) were enforced as monophyletic. The three outgroup taxa were included in the scaffold as a basal polytomy to ensure correct rooting.

Unconstrained Bayesian analysis of the matrix was carried out following the general approach of Gurovich & Beck (2009) and Travouillon *et al.* (2010). Specifically, we employed the Mk likelihood model for discrete morphological data proposed by Lewis (2001), as implemented in the program MrBayes 3.1.2 (Ronquist & Huelsenbeck 2003), with the assumption that only parsimony informative characters were scored. A gamma distribution was used to model rate heterogeneity between characters, as preliminary analyses indicated that this improved the fit of the model to the data (based on a Bayes factor value of >10; see Nylander *et al.* 2004; Gurovich & Beck 2009; Travouillon *et al.* 2010). The unconstrained Bayesian analysis comprised two independent runs of four Monte Carlo Markov chains each, of which one was 'cold' and three were 'heated' (with the temperature of the 'heated' chains set at the default value of 0.2), which were run for two million generations, sampling trees every 1000 generations. Stationarity and convergence between chains appeared to have been reached within fewer than one hundred thousand generations (based on plots of log likelihood against number of generations using the 'sump' command in MrBayes), but we conservatively excluded the first one million generations as 'burn-in'. The post-burn-in trees were summarized using 50% majority rule consensus, with Bayesian posterior probabilities as support values.

We also carried out a Bayesian molecular scaffold analysis using the general approach proposed by Worthy (2009), which involves the addition of a character block comprising multiple 'dummy' characters to enforce the monophyly of selected clades. The 'backbone' constraint topology (based on Westerman *et al.* 2012) that was used in the maximum parsimony molecular scaffold analysis (see above) was converted into a character matrix using additive binary coding, as implemented by the Perl script SuperMRP.pl (Bininda-Emonds *et al.* 2005). Under additive binary coding, each taxon is coded as '1' if it descends from a particular node in the tree and '0' if it does not, and maximum parsimony analysis of the resultant matrix will recover the topology of the original tree (this approach forms the basis of 'matrix representation with parsimony' supertrees; Bininda-Emonds *et al.* 2005). The 11 character matrix encoding the molecular scaffold was replicated 20 times, with taxa not present in the scaffold coded as unknown (i.e. '?') for all of these characters, to enforce the monophyly of clades present in the scaffold, and was then added to the morphological character matrix as a separate partition. The 74 character morphological partition and 220 character 'dummy' molecular scaffold partition were both assigned the Mk model, with a gamma distribution to model rate heterogeneity between characters and with the assumption that only parsimony informative characters were scored (i.e. as for the unconstrained Bayesian analysis), and all model parameters except tree topology were unlinked between the two partitions using the command 'unlink shape = (all) Statefreq = (all) brlens = (all)'. As a result, the 'dummy' molecular scaffold partition forces the tree topology to conform to the molecular scaffold, but does not affect other parameters (such as the shape parameter of the gamma distribution and branch lengths), which are estimated solely based on the morphological partition. The Bayesian molecular scaffold analysis was run for five million generations, of which the first four million were discarded as burn-in, but with other search parameters as for the unconstrained Bayesian analysis (see above).

Dental morphometric analysis

Although we refer all specimens described here to a single species, *B. palara*, we observed considerable qualitative variation in dental morphology within these specimens, with four distinct morphotypes present within the lower molar sample and two within the upper molar sample (see Discussion, Variation within *B. palara*). We therefore performed a bivariate morphometric analysis to determine whether the morphotypes exhibit clear and consistent differences in dental dimensions, which might be evidence that they represent different species rather than simply intraspecific variation. Upper and lower premolar and molar length and width were measured and plotted for every specimen referred to *B. palara* here, with each specimen classified as representing a particular morphotype (see Variation within *B. palara*). Other species of Riversleigh bandicoots that co-occur with *B. palara* were included in these analyses, namely *Yarala burchfieldi*, Unnamed Genus 3 sp. 1 and Unnamed Genus 5 sp. 1 and sp. 2 (see Archer *et al.* 2006; the unnamed taxa were described by Muirhead, 1994, but have yet to be formally published). Specimen numbers and measurements of these taxa are listed in Online Supplementary Material Appendix B. For each of these species, Riversleigh Faunal Zone B (= Early Miocene) and C (= Middle Miocene) specimens were labelled separately, to identify possible changes in size through time. The analysis was done using the software PAST, version 2.07.

In addition to the bivariate morphometric analysis, we also assessed variation in tooth size by calculating univariate statistics (including coefficients of variation) for dental measurements of *Bulungu palara* and seven modern bandicoot species, namely *Isoodon macrourus*, *I. obesulus*, *Perameles nasuta*, *P. gunnii*, *Echymipera clara*, *E. kalubu* and *E. rufescens*. Specimen numbers and measurements of the modern taxa are listed in Online Supplementary Material Appendix B.

Systematic palaeontology

Marsupialia (Illiger, 1811) Cuvier, 1817
Australidelphia Szalay, 1982
Order **Peramelemorphia** (Kirsch, 1968) Aplin & Archer, 1987
Superfamily incertae sedis
Family incertae sedis
Bulungu palara gen. et sp. nov.
(Figs 1–8)

Type species. *Bulungu palara* sp. nov. by monotypy.

Generic diagnosis. *Bulungu* is a small peramelemorphian (estimated body mass of ~130 g; see appendix in Travouillon *et al.* 2009 – note that *Bulungu palara* was referred to as "Peramelemorphia Genus 1 sp. 1" in that paper) that differs from all other known genera in the following combination of features: canines small; postparacrista and premetacrista contact each other just lingual to the labial margin of the tooth on M1–2, whereas these crests extend to the labial margin of the tooth without contacting each other on M3; M1 preparacrista extends posterolabially from the paracone to the base of the stylar cusp B, which is identifiable as a distinct cusp; metaconule consistently small and never as far lingual as the protocone (hence the molars are subtriangular rather than quadrilateral in occlusal outline); M3 preprotocrista terminates at the lingual base of paracone, resulting in an incomplete anterior cingulum on M3; stylar cusp B large on all molars; cristid obliqua contacts the trigonid labial to the midpoint of the metacristid on m4 only;

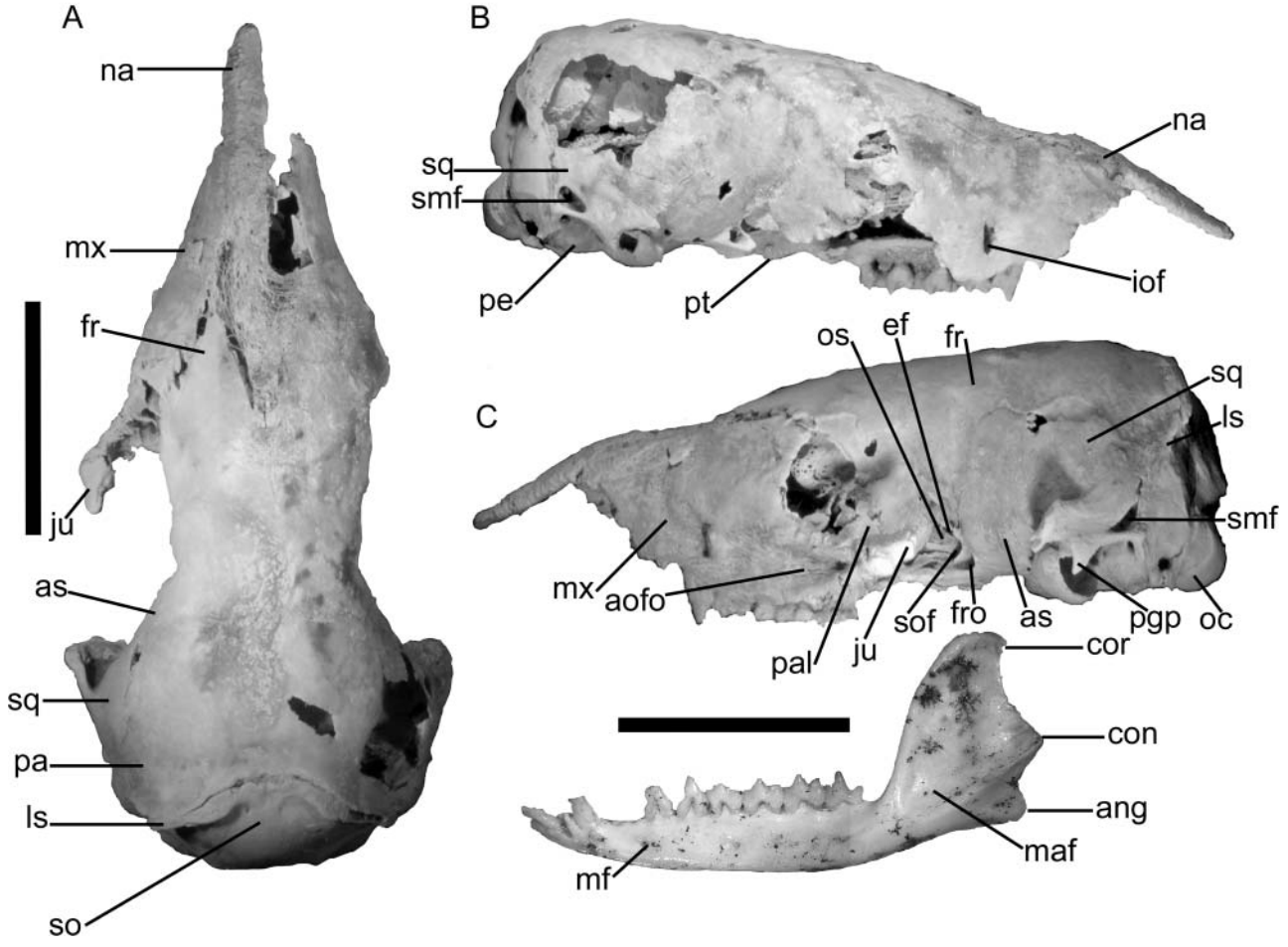

Figure 1. *Bulungu palara* gen. et sp. nov. skull (QM F23437) with dentary (QM F53025) in lateral and dorsal view. **A,** dorsal view of skull; **B,** left lateral view of skull; **C,** right lateral view of skull and left dentary in lateral view. Abbreviations: ang, angular process; aofo, anterorbital fossa; as, alisphenoid; con, mandibular condyle; cor, coronoid process; eam, external auditory meatus; ef, ethmoidal foramen; fr, frontal; fro, foramen rotundum; iof, infraorbital foramen; ju, jugal; ls, lambdoidal sesamoid; maf, masseteric fossa; mf, mental foramen; mx, maxilla; na, nasal; oc, occipital condyle; os, orbitosphenoid; pa, parietal; pal, palatine; pe, petrosal; pgp, postglenoid process; pt, pterygoid; smf, suprameatal foramen; so, supraoccipital; sof, sphenorbital fissure; sq, squamosal. Scale bar: 1 cm.

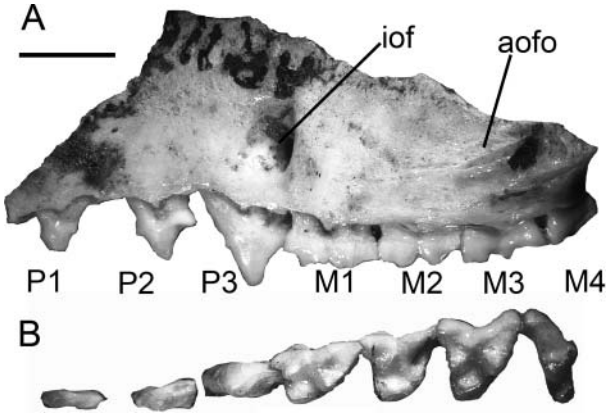

Figure 2. *Bulungu palara* gen. et sp. nov. **A,** left maxilla and **B,** upper dentition (QM F52993) in lateral view. Abbreviations: aofo, anterorbital fossa; iof, infraorbital foramen; M1–M4, upper molar one to molar four; P1–P3, upper premolar one to premolar three. Scale bar: 2 mm.

metaconid lies directly lingual to protoconid (resulting in a transverse metacristid) on all lower molars; entoconid large, with distinct pre-entocristid connecting to the base of the metaconid; hypoconulid small and positioned at the posterolingual corner of the crown; posthypocristid terminates at hypoconulid; talonid is slightly longer anteroposteriorly than the trigonid on m3; nasals extend posteriorly past the anterior margin of the orbit; two large pairs of palatal fenestrae are present in the palate posterior to incisive foramina; alisphenoid and parietal in contact on lateral wall of braincase (squamosal–frontal contact absent); the sphenorbital fissure and foramen rotundum appear elongate and tube-like, not opening directly into the endocranial cavity; primary foramen ovale very large and between the petrosal and alisphenoid; alisphenoid tympanic wing bulbous and rounded, covering the anterolateral and medial sides of the auditory recess; squamosal makes a significant contribution to the roof of the hypotympanic sinus; rostral tympanic process of the petrosal is an elongate ridge extending the length of the promontorium but without forming an enclosed sinus; epitympanic recess is relatively shallow; an arch is formed by the paroccipital and mastoid processes, exposing the region of the petrosal immediately posterior to the fenestra cochleae; rim of postglenoid foramen formed almost exclusively by squamosal, with only a small contribution by the petrosal; in posterior view, the occiput is wider than high.

Species diagnosis. As for genus diagnosis until further species are known.

Generic etymology. *Bulungu* is from the Wanyi Aboriginal word (from Riversleigh region of north-western Queensland) meaning 'sister's child' (Breen 1985), in reference to the smaller size of this animal compared to all Recent forms. Gender is considered to be feminine.

Specific etymology. The specific name, *palara*, is from the Latin palari, meaning to ramble or stray from company, in reference to its wide distribution across Riversleigh sites.

Holotype. QM F23437, partial cranium preserving left P3–M4.

Paratypes. QM F23435, right maxillary fragment with M1–3; QM F23436 left dentary with c1 p1–3 m1–4; QM F23438 left dentary fragment with m2–3; QM F23440, right maxillary fragment with P3 M1–3.

Type locality. The holotype and paratypes are all from Upper Site, Godthelp Hill, Riversleigh Station, north-western Queensland, and are part of the Upper Site Local Fauna (Archer *et al*. 1989, 1997, 2006).

Referred material. Other specimens referred here to *Bulungu palara* have been collected from the following sites at Riversleigh Station, north-western Queensland. Alan's Ledge 1990 Site (AL90): QM F54565, right dentary with p2 m1–m3; Boid Site East (BSE): QM F13103, right maxilla with M1–M4; Camel Sputum Site (CS): QM F52991, right maxilla with M3–M4; QM F52992, right dentary with c1 p1–p3 m1–m4; QM F52993, left maxilla with P1–P3 M1–M4; QM F52994, right maxilla with M2–M4; QM F52995, right maxilla with P3 M1–M4; QM F52996, left dentary with p3 m2–m4; QM F52997, right dentary with m1–m3; QM F52998, right maxilla with M1–M3; QMF 52999, right dentary with m1–m4; QM F53000, right dentary with c1 p1–p3 m1–m4; QM F53001, left maxilla with P3 M1–M3; QM F31329, right maxilla with P3 M1–M3; QM F31330, left maxilla with P2–P3 M1–M2; Dirk's Towers Site (DT): QM F24289, left dentary with c1 p1–p2 m1 m3–m4; QM F30874, right dentary with p2–p3 m1–m4; Gag Site (Gag): QM F53002, left dentary with c1, p2–p3, m2–m4; QM F53003, right dentary with m3–m4; QM F53004, left dentary with m4; QM F53005, left dentary with m3–m4; Gotham City Site (GC): QM F53006, right maxilla with M2; Henk's Hollow Site (HH): QM F53007 right dentary with p2 m1–m2; QM F53008, left dentary with m1 m3–m4; Inabeyance Site (Ina): QM F53009, left dentary with p1–p2 m3–m4; Judith's Horizontalis Site (JH): QM F53010, right dentary with m3–m4; QM F53011, left dentary with p3, m1–m2; QM F40545, right maxilla with M1–M4; Lee Sye's Outlook Site (LSO): QM F53012, right dentary with m2–m4; QM F53013 left, dentary with p3, m2–m3; Mike's Potato Patch Site (MPP or MP^2): QM F23601, left maxilla with M2–M4; Neville's Garden Site (NG): QM F53014, right dentary with m1–m2; QM F53015, left dentary with m2–m4; QM F53016, left dentary with c1 p2 m2–m4; QM F53017, left dentary with c1 p1–p2 m1–m4; QM F53018, right maxilla with M1–M4; QM F53020, right dentary with m2–m4; QM F12464, right dentary with c1, p1–p3 m1–m4; QM F24254, left maxilla with P2–P3 M1–M3; QM F24255, left dentary with p2 m2–m4; QM F24325, left dentary with m3–m4;

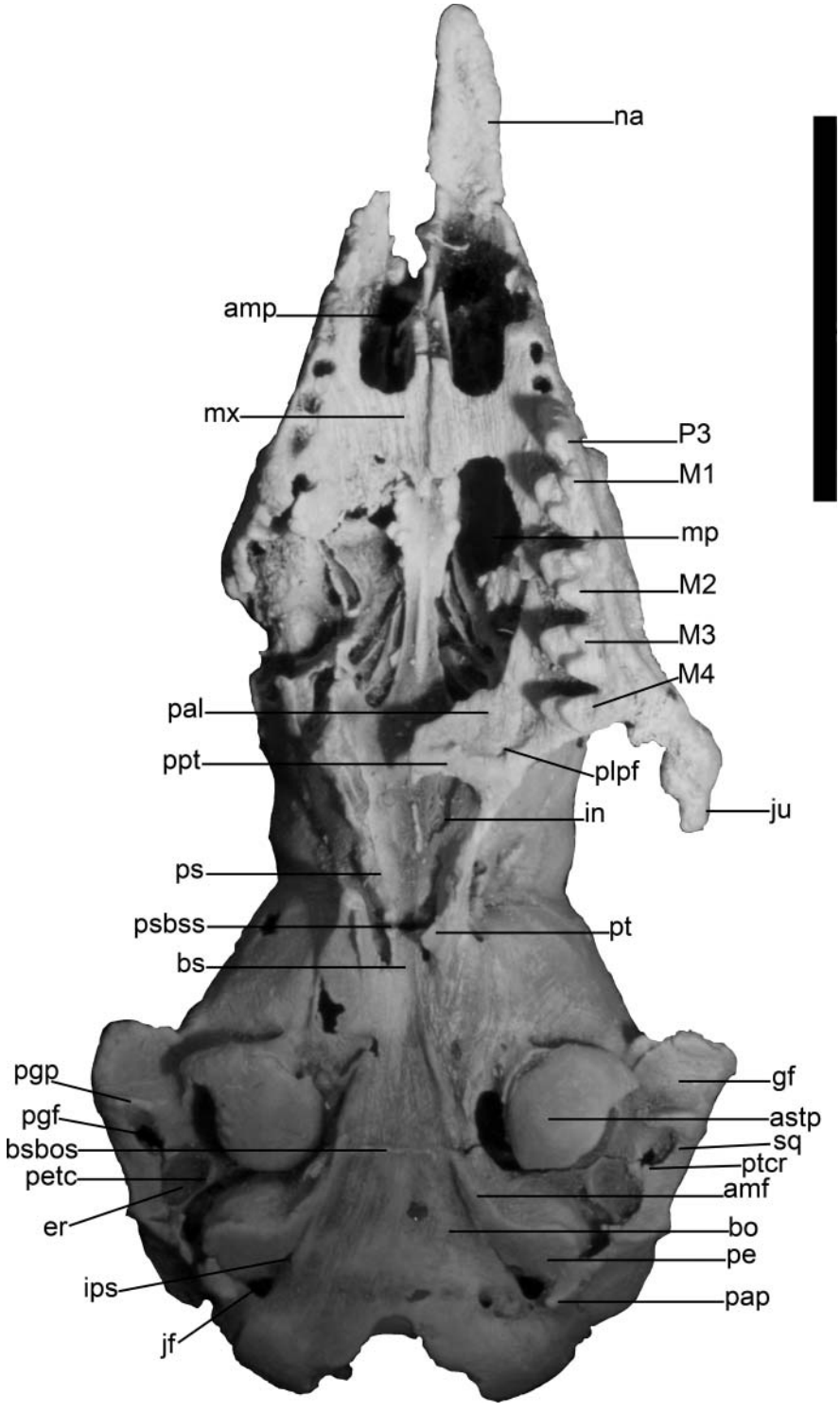

Figure 3. *Bulungu palara* gen. et sp. nov. skull (holotype QM F23437) in ventral view. Abbreviations: amf, anteromedial flange; amp, anterior maxillopalatine fenestrae; astp, alisphenoid tympanic wing; bo, basioccipital; bs; basisphenoid; bsbos, basisphenoid–basioccipital suture; er, epitympanic recess; gf, glenoid fossa; in, internal nares; ips, foramen for inferior petrosal sinus; jf, jugular foramen; ju, jugal; mp, maxillopalatine fenestra; mx, maxilla; M1–M4, upper molar one to molar four; na, nasal; pal, palatine; pap, paracondylar process of the exoccipital; pe, petrosal; petc; petrosal crest; pgf, postglenoid foramen; pgp, postglenoid process; plpf, posterolateral palatal foramen; ppt, postpalatine torus; ps, presphenoid; psbss, presphenoid–basisphenoid suture; pt, pterygoid; ptcr, post-tympanic crest; P3, upper third premolar one; sq, squamosal. Scale bar: 1 cm.

QM F30732, right dentary with p1 m1–m3; QM F30733, left dentary with m1–m3; QM F31452, skull fragment with right C1 P3 M2; Outasite (Out): QM F53022, left maxilla with M1–M2 M4; Price is Right Site (PIR): QM F53024, left dentary with m1–m2; Rat Vomit Site (RV): QM F53025, left dentary with c1 i1 i3 p2–p3 m1–m4; Rick's Sausage Site (RS): QM F 54566, right dentary with p1–p3 m1–m2; Ringtail Site (Ring): QM F23549, right dentary with P3 M2–M4; Ross Scott-Orr Site (RSO): QM F53026, right dentary with m3–m4; QM F53027, right maxilla with M2–M4; QM F53028, right maxilla with M1–M4; QM F53030, left dentary with p1–p3 m1–m4; QM F53031, left maxilla with M2–M4; QM F53032, right dentary with m2–m3; Two Trees Site (TT): QM F54562, left dentary with c1 p1–p3 m1–m4; Upper Site (U): QM F53033, left dentary with m1–m4; QM F53034, left maxilla with M3–M4; QM F53035, right dentary with m3–m4; QM F53037, left dentary with p2–p3 m1–m4; QM F53038, left dentary with m3–m4; QM F53039, right dentary with p3; QM F53042, left dentary with p2–p3 m1–m4; QM F53043, left maxilla with M3–M4; QM F53589 left dentary with p2–p3 m1–m4; QM F53616, right maxilla with M2–M3; QM F53627, left dentary with m3; QM F53614, left maxilla with M2–M4; QM F53633, left maxilla M1–M4; QM F53615, left maxilla with M2–M4; QM F53599, right maxilla with P2–P3 M1–M3; QM F53591, right dentary with p3 m1–m4; QM F53583, right dentary with m1–m4; QM F53604, left dentary with m3–m4; QM F53628, left maxilla with M1–M3; QM F53622, right maxilla with M2; QM F53613, right maxilla with P2; QM F53605, right maxilla with M3; QM F53593, left dentary with c1 p1–p3 m1–m4; QM F54600, left maxilla with M2–M3; QM F53590, left dentary with m2–m4; QM F53632, right maxilla with m1–m2; QM F53618, right maxilla with M2; QM F53610, left maxilla with P1–P2 M1; QM F53620, right maxilla with M1–M2; QM F53586, right maxilla with C1 P1–P3 M1–M4; QM F53634 left dentary with p2–p3 m1–m4; QM F53621, left dentary with m3–m4; QM F53585, right dentary with p2 m1–m4; QM F53606, right maxilla with M3; QM F53592, right dentary with p2–p3 m1, m3–m4; QM F53624, right maxilla with M3; QM F53594, left maxilla with M3; QM F53626, right maxilla with P3 M1–M4; QM F53588. left maxilla with P2–P3 M1–M3; QM F53584, right maxilla with P3 M1–M3; QM F53597, right dentary with m3; QM F53587, left dentary with p2 m3–m4; QM F53602, right dentary with m3–m4; QM F53601, right maxilla with P3 M1–M4; QM F53608, left maxilla with M1–M2; QM F53612, left maxilla with P3 M2–M4; QM F53603, left maxilla with M2–M3; QM F53596, left maxilla with M2–M4; QM F53607, right maxilla with M2–M4; QM F53602, right maxilla with P3 M1–M4; QM F53630, left dentary with m1–m2; QM F53598, right maxilla with M1–M2; QM F20791, right maxilla with M1–M3; Wang Site (Wang): Q MF52990 left dentary with m3–m4; QM F53582, left maxilla with M2–M3; QM F24596, left dentary with m1–m4; QM F36397, right maxilla with M2–M4; Wayne's Wok Site (WW): QM F53565, left dentary with m3–m4; QM F53567, left maxilla with M2–M4; QM F53568, right dentary with m3; QM F53569, left dentary with m1–m3; QM F53571, left dentary with m3–m4; QM F53572, right dentary with m3; QM F53573, left dentary with m3–m4; QM F53576, right maxilla with M3–M4; QM F53577, right maxilla with P2–P3 M1; QM F53578, left maxilla with M3; QM F53579, left maxilla with M1–M3; QM F53563, right maxilla with M2–M3; QM F24551, left dentary with m3–m4.

We also identify the presence of *Bulungu palara* in the Early–Middle Miocene Leaf Locality of the Kutjamarpu

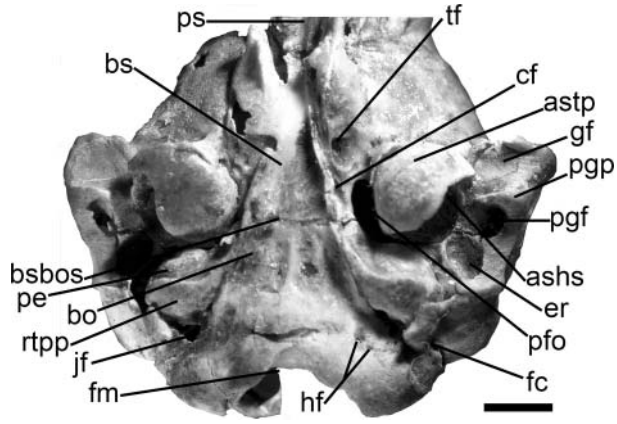

Figure 4. Detailed view of *Bulungu palara* gen. et sp. nov. basicranium (holotype QM F23437). Abbreviations: ashs, alisphenoid hypotympanic sinus; astp, alisphenoid tympanic wing; bo, basioccipital; bs; basisphenoid; bsbos, basisphenoid–basioccipital suture; cf, ceratoid foramen; er, epitympanic recess; fc, fenestra cochleae; fm, foramen magnum; gf, glenoid foramen; hf, hypoglossal foramina; jf, jugular foramen; pe, petrosal; pfo, primary foramen ovale; pgf, postglenoid foramen; pgp, postglenoid process; ps, presphenoid; rtpp, rostral tympanic process of the petrosal; tf, transverse foramen. Scale bar: 2 mm.

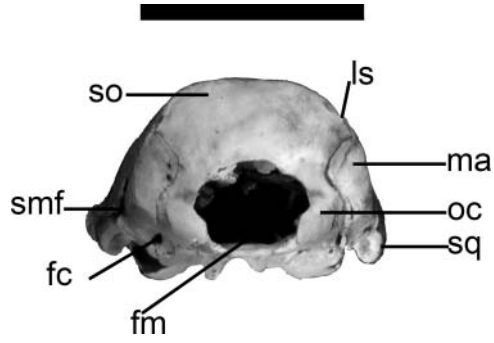

Figure 5. Detailed dorsal view of *Bulungu palara* gen. et sp. nov. skull (holotype QM F23437). Abbreviations: fc, fenestra cochleae; fm, foramen magnum; ls, lambdoidal sesamoid; ma, mastoid; oc, occipital condyle; smf, suprameatal foramen; so, supraoccipital; sq, squamosal. Scale bar: 1 cm.

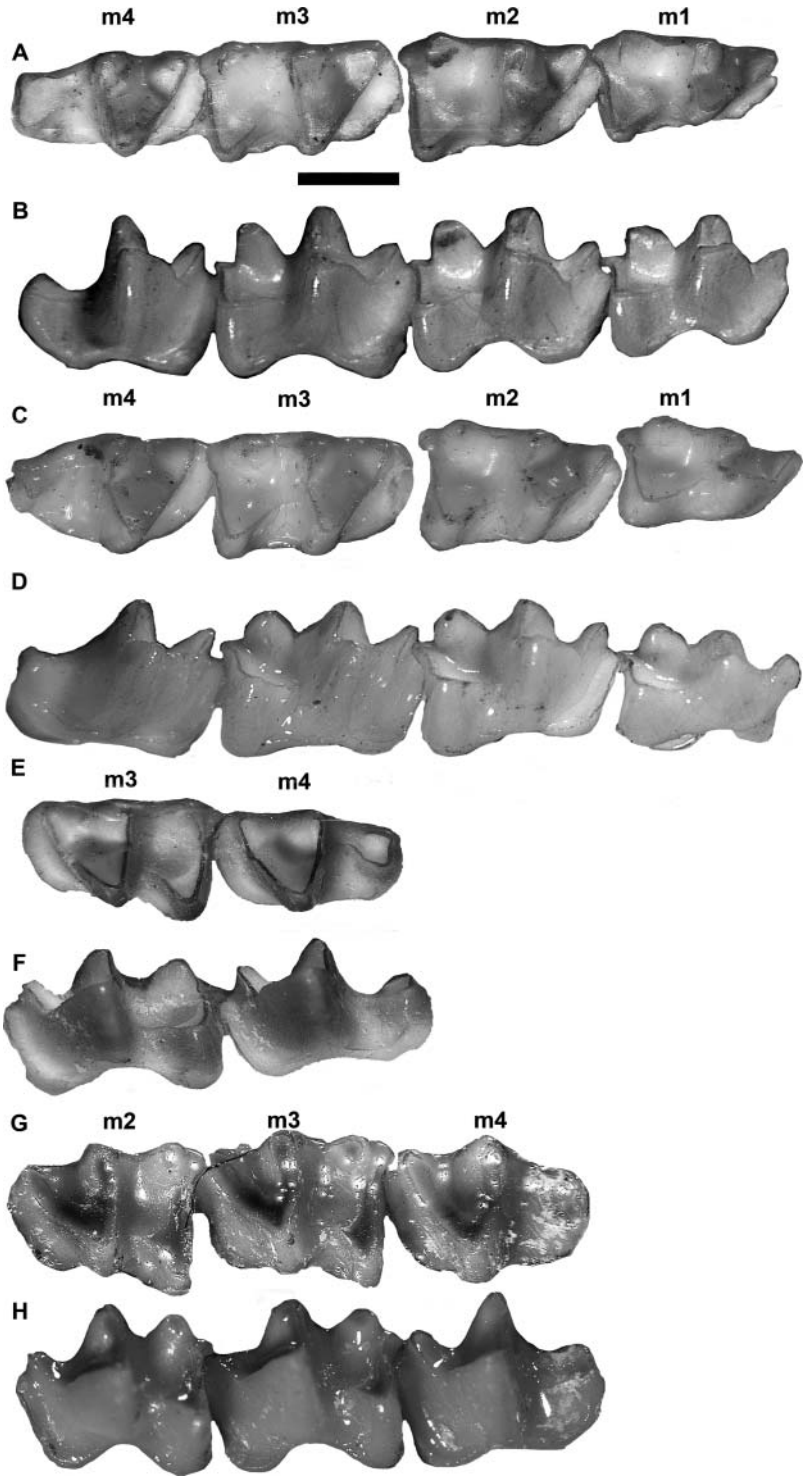

Figure 6. Morphological variation of lower teeth of *Bulungu palara* gen. et sp. nov. from Riversleigh. **A,** occlusal view of morphotype L1 (QM F52992, right dentary c1, p1–p3, m1–m4) from Camel Sputum site in Faunal Zone B; **B,** labial view of right dentary (QM F52992); **C,** occlusal view of morphotype L2 (QM F24289 right dentary c1, p1–p3, m1–4) from Dirk's Tower site in Faunal Zone B; **D,** labial view of right dentary (QM F24289); **E,** occlusal view of morphotype L3 (QM F52990, left dentary m3–m4) from Wang Site in Faunal Zone C; **F,** labial view of left dentary (QM F52990); **G,** occlusal view of morphotype L4 (QM F53002, left dentary c1, p2–p3, m2–m4) from Gag Site in Faunal Zone C; **H,** labial view of left dentary QM F53002. Scale bar: 1 mm.

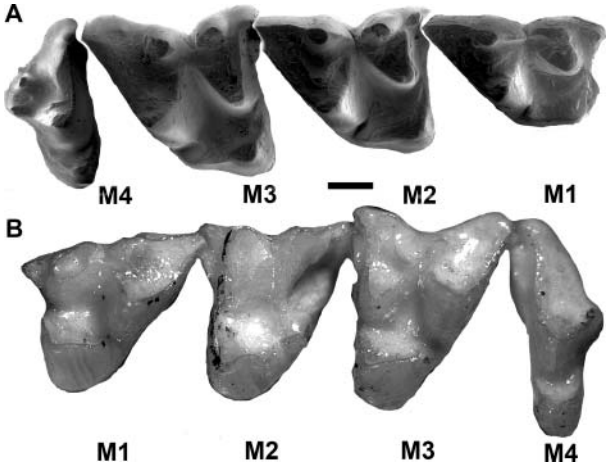

Figure 7. Morphological variation of upper teeth of *Bulungu palara* gen. et sp. nov. from Riversleigh. **A,** occlusal view of morphotype U1 (QM F53586, right maxilla with (C1, P1–P3 not pictured), M1–M4) from Upper Site in Faunal Zone B; **B,** occlusal view of morphotype U2 (QM F52993 left maxilla with (P1–P3 not pictured, M1–M4) from Camel Sputum site in Faunal Zone B. Scale bar: 0.5 mm.

LF, Wipajiri Formation, Lake Ngapakaldi, Tirari Desert, Lake Eyre Basin, South Australia (Woodburne *et al.* 1993; Travouillon *et al.* 2006), based on two specimens, namely: and SAMP 66837, left dentary with m2 and m3 and SAMP 108072, right M2. A complete list of specimens and their associated dental measurements is given in Online Supplementary Material Table 1 (lower dentition) and Online Supplementary Material Table 2 (upper dentition).

Age. The age of the Riversleigh fossil localities is based on biocorrelation with other Australian Oligo-Miocene fossil localities. Four distinct 'Faunal Zones' (FZs) have been identified, each proposed to represent a different time period (Archer *et al.* 1989, 1997; Arena 2004; Travouillon *et al.* 2006, 2011): FZA appears to be Late Oligocene in age, while FZB is Early Miocene, FZC is Middle Miocene, and FZD is early Late Miocene. Riversleigh specimens of *Bulungu palara* are from the Late Oligocene FZA (LSO and Quantum Leap Site [QL]), the Early Miocene FZB (BSE, CS, DT, Ina, JH, MPP, NG, Out, PIR, RV, RSO, U and WW), and the Middle Miocene FZC (AL90, Gag, GC, HH, Ring, TT and Wang). Given that only a few taxa are currently known from RS, it is unclear to which Faunal Zone it belongs (Travouillon *et al.* 2011); however, based on its close geographical proximity to AL90, it may be FZC.

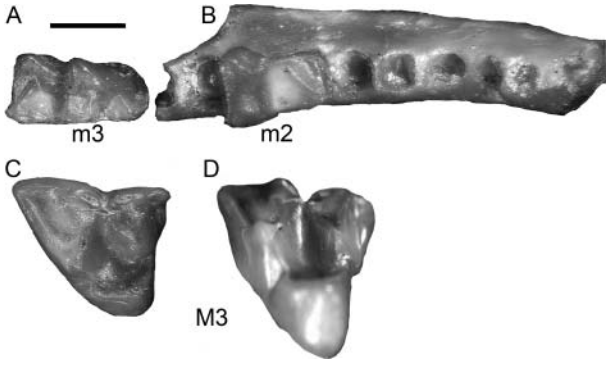

Figure 8. *Bulungu* sp. cf. *B. palara* gen. et sp. nov. from the Kutjamarpu Local Fauna, (Wipajiri Formation), Lake Eyre Basin, South Australia. **A,** left m3 corresponds to the left dentary (SAM P66837) in occlusal view; **B,** left dentary with left m2 in place (SAM P66837); **C,** isolated right M3 (SAM P108072) in occlusal view; **D,** isolated right M3 (SAM P108072) in lingual view. Scale bar: 1 mm.

The Kutjamarpu LF is found in the Wipajiri Formation, the age of which remains uncertain. Megirian *et al.* (2010) placed the Kutjamarpu LF within their 'Wipajirian' Australian Land Mammal Age, which they estimated as spanning from 24.9–24.6 Ma (i.e. Late Oligocene) to ?17.6 Ma (i.e. Early Miocene; Megirian *et al.* 2010, table 2). However, according to Megirian *et al.* (2010), the base of the Wipajirian is within the Etadunna Formation, between Etadunna Faunal Zones B (the Ditjimanka Local Fauna) and C (the Ngapakaldi Local Fauna). Between the base of the Wipajarian *sensu* Megirian *et al.* (2010) and the Kutjamarpu LF (which is within the Wipajiri Formation, which lies unconformably over the Etadunna Formation), are Etadunna Faunal Zones C and D, a hiatus, Etadunna Faunal Zone E, and then a second hiatus (Woodburne *et al.* 1993). Metzger & Retallack (2010) analysed a 35 m section of a drill core from Lake Palankarinna and used a best-fit age-model to estimate an age range of 26.1–23.6 Ma for the Etadunna Formation. If this age range is correct, then the Kutjamarpu LF must be younger than 23.6 Ma, although exactly how much younger is dependent on the length of the hiatus between Etadunna Faunal Zone E and the Wipajiri Formation. Unless this hiatus was very short, and the Wipajiri Formation represents only a very short period of deposition, then the Kutjamarpu LF is almost certainly Miocene in age.

The minimum age for the Wipajiarian given by Megirian *et al.* (2010, table 2), namely ?17.6 Ma, is also problematic. This date is based on the shared presence of wynyardiids between the Tasmanian Wynyard LF (dated as 21.0–17.6 Ma based on foram data; Macphail 1996) and the Kutjamarpu LF (Megirian *et al.* 2010, p. 668). However, wynyardiids are also known from the older 'Etadunnan' *sensu* Megirian *et al.* (2010; Pledge 1987, 2003), and so their presence in both the Wynyard and Kutjamarpu LFs is not evidence that they are contemporaneous. In addition, the only wynyardiid (indeed, the only mammal) specimen from the Wynyard LF, the holotype of *Wynyardia bassiana*, does not preserve any part of the dentition, making comparisons with other wynyardiid taxa difficult and probably precluding the use of stage-of-evolution biocorrelation, as for mammals this is usually based on dental characters. A

more conservative minimum age would be based on the age of the Bullock Creek LF, which is universally accepted to be younger than the Kutjamarpu LF, and is estimated to be Middle Miocene in age ('Camfieldian' *sensu* Megirian *et al.* 2010), although a more precise age is currently unavailable. In summary, the Kutjamarpu LF appears to be younger than 23.6 Ma, but older than the Middle Miocene Bullock Creek LF, and therefore is probably Early–Middle Miocene in age, in agreement with previous estimates based on biocorrelation (Rich *et al.* 1991; Travouillon *et al.* 2006). Most recently, an Early–Middle Miocene age for the Kutjamarpu LF was also supported by Black *et al.*'s (2012) biostratigraphical analysis of the diprotodontid *Neohelos*, these authors suggesting that it lies between Riversleigh FZB and FZ C in age.

Description

Nasal. The anterior part of the left nasal bone is intact, whereas the right is missing entirely (see Fig. 1A, B). The preserved part of the left nasal is thin and straight, and its overall proportions indicate that the rostrum of *Bulungu palara* was proportionally short compared to those of Recent bandicoots (see Palaeoecology below). Posteriorly, the nasals terminate behind the anterior margin of the orbital fossa. The nasal sutures are parallel anteriorly and widen only slightly in the molar region.

Maxilla. The maxilla is incomplete on both sides in QM F23440, but is more complete on the left side. The left maxilla is intact from the level of P3 back, and gradually widens posteriorly. The facial process of the maxilla contacts the jugal posterolaterally along a distinctly v-shaped suture, the jugal subdividing into distinct dorsal and ventral processes at its anterior end. Ventrally, the maxilla is incomplete due to damage to the palate, and the incisive foramina are not preserved. The 'accessory' palatal fenestrae *sensu* Voss & Jansa (2009) are wide, taking up nearly the entire width of the palate. Posterior to this, there is a second pair of palatal vacuities developed within the maxillopalatine suture (i.e. maxillopalatine palatal fenestrae *sensu* Voss & Jansa 2003, 2009), extending from level with the posterior root of P3 to approximately level with M4. Both left and right maxillopalatine fenestrae are damaged (although the left fenestra is considerably more intact), and it is unclear whether a complete dividing septum was originally present or not. There are no additional vacuities between the maxillopalatine fenestrae and the posterior margin of the palate, i.e. palatine fenestrae *sensu* Voss & Jansa (2003) are absent.

Infraorbital canal. The infraorbital foramen is dorsal to P3 (see Fig. 1B, C) and is entirely enclosed by maxilla. A small groove (most likely a foramen filled with remaining limestone matrix) is identifiable within the opening of the infraorbital foramen, and is probably the opening for the incisivomaxillary canal that transmitted nerves and blood vessels to the anterior dentition (Evans 1993). The maxillary foramen (the posterior opening of the infraorbital canal, within the orbital fossa) is incomplete due to loss of the lacrimal, but the infraorbital canal is clearly long, extending from level with the posterior crown tip of P3 to the posterior crown tip of M3 (as in *Yarala burchfieldi*). This is in contrast to the shorter infraorbital canal of *Galadi speciosus*, which extends from the posterior root of P3 to the posterior crown tip of M2.

Palatine. In lateral view, the palatine consists of two processes, a triangular process that extends anteriorly to contact the frontal, and a smaller, narrower process that extends posteriorly to contact the alisphenoid. The suture between the palatine and alisphenoid is v-shaped. Dorsal to the palatine–alisphenoid suture, the palatine is in contact with the frontal. The large, oval sphenopalatine foramen lies within the anterior process of the palatine, at the intersection of the lateral wall of the cranium and the horizontal floor of the orbital fossa (Fig. 1C). The palatine extends laterally and ventrally, making a small contribution to the horizontal floor of the orbital fossa (at the anterior end of the zygomatic arch), and contacting the maxilla.

Posterolateral palatal foramen. Posterior and slightly ventral to the sphenopalatine foramen, the posterolateral palatal foramen (Voss & Jansa 2003) is present at the posterior end of the maxillopalatine suture in the palate (Fig. 3). This foramen is complete and is an elongate oval in outline; a thin process of maxilla forms the anterior part of the margin, while a thin process of the palatine forms the posterior part, as in *Galadi* (Travouillon *et al.* 2010).

Palate. Ventrally, the palatine and maxilla meet in the palate (see Fig. 1C). The remnants of the suture between the maxilla and palatine are visible on the left side of the skull. This suture begins at the base of the maxillopalatine fenestra and extends posteriorly from the posterolateral corner of the fenestra, forming an n-shape. A narrow, deep posterolateral palatal foramen (Fig. 3) is present beneath the transverse palatine process (bar) on the maxillopalatine suture. The transverse palatine process (bar) is damaged but partly preserved on the left side and has a distinct round edge.

Lacrimal. Both lacrimals are missing, and hence the presence or absence of a lacrimal crest (the presence of which is characteristic of the Recent Australian genera *Isoodon*, *Perameles*, *Macrotis* and *Chaeropus*, but which is absent in peroryctids (Muirhead 1994), cannot be determined (Fig. 1B, C).

Zygomatic arch. The left zygomatic arch is incomplete but the anterior and posterior roots are preserved, whilst only the posterior root of the right zygomatic arch is present.

Anteriorly, the maxillojugal suture is v-shaped, with the jugal subdividing into distinct dorsal and ventral processes at its anterior end, as in other peramelemorphians (see Muirhead 2000; Travouillon *et al.* 2010). The antorbital fossa between the dorsal and ventral process of the jugal is shallow (see Fig. 2) compared to most extant peramelemorphians but slightly deeper than in *Microperoryctes longicauda*, *Isoodon obesulus*, *Galadi speciosus* (see Travouillon *et al.* 2010) and *Yarala burchfieldi* (see Muirhead & Filan 1995). At the posterior root of the zygomatic arch, a reinforced floor is present composed of both the alisphenoid and squamosal.

Frontal. In dorsal view, the paired frontals are v-shaped anteriorly, contacting the nasals (dorsally) and the maxilla (laterally; see Fig. 1A). The frontal contact with the maxilla (preserved on the left side only) is saw-shaped, as in *Galadi* (see Travouillon *et al.* 2010). Laterally, the anterior margin of the frontal would have contacted the lacrimal (which is missing from both sides of the skull), and posteroventrally it makes a straight contact with the palatine and the dorsal edge of the orbitosphenoid. At its posterior margin, the frontal contacts the parietal (dorsally) and the alisphenoid (ventrolaterally). The contact with the parietal is a straight suture, which becomes slightly sinuous and wavelike medially. Viewed dorsally, the frontal is at its widest at the anterior margin of the orbits, just posterior to the point of contact between the lacrimal, maxilla and frontal. The skull narrows anterior to the alisphenoid–frontal suture on the dorsal and lateral sides and then flares out at the region of contact between the parietal, alisphenoid and squamosal.

Parietal. The parietal is roughly square in shape, contacting the frontal dorsoanteriorly, the alisphenoid and squamosal ventrally, and the mastoid posteriorly. The mastoid–parietal suture reaches the same dorsal level as the alisphenoid–parietal suture. There is no sagittal crest on either the frontal or parietal.

Cranial floor. In ventral view, the cranium pinches in and narrows posterior to the palate. The posterior opening of the internal nares is damaged; the left side is more complete and indicates that the opening was heart-shaped and wide. It is not possible to determine if there was a dividing septum of the internal nares. The presphenoid is visible due to damage to the pterygoids (the left pterygoid is better preserved than the right), and is in lateral contact with the pterygoids. There is a clear gap between the presphenoid and basisphenoid. There are two long oval foramina (the right of which is damaged, but the left of which is intact) present on the lateral wall on each side of the presphenoid–basisphenoid suture, and these foramina open respectively into the left and right sphenorbital fissure. These foramina are not observed in *Galadi.*

The basisphenoid is narrow anteriorly but expands posteriorly (Fig. 3). It forms a raised lateral edge (which is better preserved on the right side than on the left) that is in contact with the alisphenoid. Along the floor of the basisphenoid there is a slight narrow ridge present on the midline and this continues on to the basioccipital. On either side of this narrow ridge, the floor of the basisphenoid is slightly depressed and concave, and this continues posteriorly past the basisphenoid–basioccipital suture and onto the basioccipital. These bilateral concavities probably represent the attachment of the medial part of the longus capitis muscle (see Filan 1990, p. 632), and are deeper in the basioccipital than in the basisphenoid. The basioccipital is narrow at the basisphenoid–basioccipital suture, but widens posteriorly towards the foramen magnum.

Ventrally, two foramina are observed within the suture between the petrosal and basioccipital: the smaller, more anterior foramen is for the inferior petrosal sinus, while posterior to this is the larger jugular foramen (see Fig. 3). Both foramina are formed by notches on the lateral ridge of the basioccipital and notches on the medial wall of the petrosal. Anterior to the occipital condyle, the paired hypoglossal foramina (Fig. 4) are present, with the more posterior of the foramina also slightly lateral to the anterior foramen. The paroccipital processes are relatively tall, wide and ventrally directed. They contact the mastoid process of the petrosal. The foramen magnum (Fig. 4) has a distinct, wide notch (incisura occipitalis) in the dorsal margin (see Voss & Jansa 2009, fig. 13).

Alisphenoid. The paired alisphenoid bones make a large contribution to the lateral wall of the braincase of the skull (Fig. 1C). The alisphenoid contacts the parietal dorsally and prevents contact between the squamosal and frontal (Fig. 1A), as in the fossil peramelemorphians *Yarala* and *Galadi*, but unlike all Recent peramelemorphians in which the frontal and squamosal are in contact. The alisphenoid–frontal contact is long, whereas the alisphenoid–parietal suture is short and vertical. Laterally, the alisphenoid–squamosal suture is vertical and extends directly to the posterior root of the zygomatic arch, as in *Galadi* (Travouillon *et al.* 2010). In dorsal view, the alisphenoid forms the anteromedial part of the posterior root of the zygomatic arch and thus an entoglenoid process of the alisphenoid *sensu* de Muizon (1998) is present. In lateral view, the foramen rotundum can be identified within the alisphenoid, posterior and slightly ventral to the orbitosphenoid. The opening of the foramen rotundum is approximately the same size and shape as the sphenorbital fissure, from which it is separated by a thin wall of bone.

Alisphenoid tympanic wing. The alisphenoid tympanic wing is bulbous and rounded, but is open laterally. It encloses the hypotympanic sinus. The alisphenoid tympanic wing (Fig. 4) is more rounded and complete on the left side,

and may be slightly broken or damaged on the right side, where it is distorted and pushed in towards the braincase. The left alisphenoid tympanic wing terminates in the region level with the posterior edge of the postglenoid foramen (see Fig. 4); the right alisphenoid tympanic wing is more damaged and slightly flattened, but terminates more posteriorly, posterior to the posterior edge of the postglenoid foramen and closer to the right petrosal.

Orbitosphenoid. The orbitosphenoid is a small paired bone exposed on the lateral orbital wall, similar in size to *Yarala burchfieldi*; by contrast, the orbitosphenoid is much smaller or hidden in lateral view in most Recent bandicoots (Muirhead 2000; Travouillon *et al.* 2010). There are two ethmoidal foramina (Fig. 1C): one is located at the posterodorsal corner of the orbitosphenoid, within the suture between this bone and the frontal, and probably transmitted the external ethmoidal artery and vein; anterior to this foramen is a second ethmoidal foramen, which is small, oval and probably transmitted the ethmoidal nerve (see Wible 2008, pp. 339–340). The sphenorbital fissure lies immediately posterior to the orbitosphenoid, between the orbitosphenoid and the alisphenoid. The cranium is at its narrowest at the level of the orbitosphenoid, with an indentation in the frontal on each side which is pronounced in dorsal view, giving the skull a 'pinched in' appearance (see Fig. 1A).

Squamosal. The squamosal forms the posterior part of the zygomatic arch (Fig. 1C). Laterally, the squamosal–alisphenoid suture runs almost perpendicular to the parietal. The squamosal does not contact the frontal. Dorsally, the squamosal has a long, almost horizontal contact with the parietal. The suprameatal foramen (Wible 2003) or subsquamosal foramen of Archer (1976) is observed dorsal to the external auditory meatus, posterodorsal to the postglenoid process. It is partially damaged on the left hand side and preserved on the right hand side of the skull. It is large and slightly bean-shaped on the right hand side (Fig. 1C).

Auditory region. The alisphenoid makes a very small contribution to the anteromedial margin of the glenoid fossa, representing an alisphenoid glenoid process/entoglenoid process of the alisphenoid (see Fig. 3). The glenoid fossa is deep with raised pre- and post-glenoid processes. The squamosal extends onto the cranium medial to the glenoid fossa (Fig. 4). The transverse foramen is large and circular (Fig. 4) and located within the alisphenoid, lateral to the ridge-like contact between the alisphenoid and basisphenoid. The carotid foramen (entocarotid foramen of Archer 1976) is oval in shape, larger than the transverse foramen and located directly posterior to the transverse foramen. The carotid foramen (Fig. 4) is separated from the primary foramen ovale laterally by a thick wall of the alisphenoid. A distinct carotid canal is present, forming a trough extending anteriorly on the basisphenoid lateral crest and leading into the carotid foramen. The carotid foramen lies directly anterior to the petrosal.

The primary foramen ovale (Fig. 4) is large and lies directly lateral to the carotid foramen. It is mostly surrounded by the alisphenoid, with the lateral margin formed by the base of the tympanic bulla, but the posterior margin is formed by the petrosal. The primary foramen ovale is widest anteriorly and narrows posteriorly. Lateral to the transverse foramen, at the base of the alisphenoid tympanic process, there are three foramina. The largest of these foramina is on the base of the alisphenoid tympanic process (Fig. 4). The other two smaller circular foramina are anterior to the base of the alisphenoid tympanic process. On the right hand side of the skull, only two large foramina are observed. None of these openings appear to open directly into the endocranial space. These foramina resemble the foramina for the buccinator and masseteric nerves seen in some Recent peramelemorphians, such as *Peroryctes broadbenti* and *P. raffrayana* (see Aplin *et al.* 2010, fig. 8). The ectotympanic is not preserved on either the right or left sides.

Postglenoid foramen. The postglenoid foramen is large, with the squamosal forming the anterolateral wall of the foramen. The suture between the squamosal and petrosal occurs at the posteromedial corner of the postglenoid foramen, and hence the petrosal forms the posteromedial margin of the postglenoid foramen, as in *Galadi* (Travouillon *et al.* 2010). The posteromedial border of the postglenoid foramen borders the epitypmpanic recess (Fig. 4); there is no distinct wall or ridge separating the postglenoid formamen from the epitympanic recess as is seen in *Galadi*, but this may be due to damage in the region.

The region of the squamosal between the postglenoid process and postympanic process is deeply concave and provides the major opening into the ear region (external auditory meatus). The squamosal flattens into a slight depression at the base of the post-tympanic process; in lateral view this depression is identifiable as a small but distinct concavity which may represent a small squamosal epitympanic sinus, as in *Galadi* (Travouillon *et al.* 2010).

Petrosal. The pars cochlearis of the petrosal is comma-shaped when viewed ventrally and has a bulbous promontorium (Fig. 4); however, it is relatively flat anteriorly, lateral to the primary foramen ovale and alisphenoid tympanic wing. The petrosal does not overlap the basioccipital. The anterior region of the petrosal (anteromedial flange *sensu* Wible 2003) is slightly convex laterally and extends as far as the basisphenoid–basioccipital suture.

The rostral tympanic process of the petrosal is visible as a raised ridge that extends the full length of ventral surface of the promontorium (Fig. 4). The fenestra cochlea is posteromedial to the fenestra vestibuli. On the ventral edge of the petrosal, there is a thick wall separating both fenestrae. The

fenestrae are similar in size and are circular. The fenestra cochleae is not fully visible in ventral view; instead, it is hidden by a wall formed by the mastoid and the paroccipital process of the exoccipital, which contact each other at their ventralmost extremities, enclosing a distinct foramen the leads to the fenestra cochleae when viewed posteriorly. There is a stylomastid notch for the exit of the facial nerve (rather than a complete foramen), as in *Galadi* (see Travouillon *et al.* 2010) and all other peramelemorphians. Anterior and lateral to the fenestra vestibuli is the small secondary facial foramen (only visible on the left side).

Anteromedial to the promontorium, the petrosal makes a small contribution to the roof of the hypotympanic sinus. Lateral to the promontorium and lateral to the fenestra vestibuli are two sinuses or concavities within the anterior lamina of the petrosal (*sensu* Ladevèze 2004), the more anterior of which is the deeply excavated epitympanic recess (Fig. 4) and the more posterior is the fossa incudis, which is not particularly well defined.

The epitympanic recess is separated from the petrosal contribution to the hypotympanic sinus by a distinct lateral crest (the lateral malleolar ridge *sensu* Aplin 1990; the petrosal crest *sensu* Archer 1976). The epitympanic recess (Fig. 4) is similar in depth to that of *Galadi* (whereas it is slightly deeper in *Yarala*) and its anterior wall forms the posteromedial margin of the postglenoid foramen.

In posterior/occipital view (Fig. 5) the mastoid is rectangular in shape, forming a vertical anterior contact with the squamosal; this suture continues dorsally to contact with the parietal.

Occipitals. In ventral view, no suture marking the boundary between the exoccipitals and basioccipital is identifiable. The ventral portion of the basioccipital is relatively flat except for a low middle ventral ridge and a higher lateral ridge formed where the basioccipital abuts the petrosal, which encloses the inferior petrosal sinus (this is also observed in *Galadi*; see Travouillon *et al.* 2010). The occipital condyle is rounded but does not extend ventrally below the level of the horizontal plane of the basioccipital. There is a pair of hypoglossal foramina within the basioccipital on both sides of the skull (Fig. 4).

Posterior cranial wall. The exoccipitals and supraoccipital (Fig. 5) are fused and hence no suture between these bones can be identified. The foramen magnum and the posterior cranial wall as a whole (see Fig. 5) are both wider than high. The dorsolateral corners of the posterior cranial wall are marked by lambdoid crests. Sesamoids are present as distinct thickenings within the lambdoidal crests (Fig. 1A).

The supraoccipital is curved dorsally and contributes to the posterodorsal roof of the skull. The posterior cranial wall in the region of the mastoid is poorly distinguished from the lateral cranial wall due to the curved mastoids. On either side, the lambdoid crest continues into the dorsal region of the mastoid but terminates in the region of contact with the squamosal. The supraoccipital and posterior cranial wall as a whole are convex and bulbous. The occipital condyles are rounded and protrude outwards slightly beyond the foramen magnum.

Dentary. The left dentary of QM F23436 is nearly complete except for a broken mandibular condyle, and hence our description of the dentary is largely based on this specimen. The mandibular symphysis is elongate, extending back to m1. The masseteric fossa is deep. There are two small mental foramina present, one below p1 and one below m1. However, there is some variation in the position of the anterior mental foramen between specimens: in QM F52992, it lies between p1 and p2 rather than below p1, whereas it is directly under the anterior root of p2 in QM F53025.

The coronoid process forms an approximate angle of 100° with the dental ramus. The mandibular ramus is at its greatest depth below m2–m3 and is approximately twice the crown height of that molar (see Fig. 1C). The dentary is proportionately shorter than that of Recent peramelemorphians.

Lower dentition. The lower dentition is based on QM F53025 and QM F52992 (Fig. 6A, B). Two lower incisors are preserved in QM F53025: i1 is broken at the tip, whereas i2 is spade-shaped and procumbent. The third incisor is missing and therefore it cannot be determined whether it was bi-lobed, but its alveolus is preserved. The alveolus of i2 is staggered relative to those of i1 and i3 (Hershkovitz 1982, 1985). In QM F53025, c1 is broken and only the lower half of the canine remains. In QM F52992, a complete canine is present and is approximately twice as tall as p1. A diastema is present between c1 and p1 (QM F23436 and QM F52992).

The p1 is separated from p2 by a small diastema, but no diastema is present between p2 and p3, and the crowns of p3 and m1 are in direct contact. Two cusps are present on p1, of which the larger is anteriorly positioned and connected to the smaller posterior cusp by a long crest. The p2 is larger than p1, but the two teeth are similar in overall morphology except that an additional small anterior cusp is present on p2. The main central cusp of p2 curves lingually, and the posterior region of the main cusp widens labiolingually.

The morphology of p3 is similar to p2 except that the anterior of the three cusps is larger and more distinct. The crown of p3 is higher than that of p2, but this is due to the roots having erupted well above the alveolar margin of the dentary, especially the anterior root, which has caused the crown to incline posteriorly towards m1; this morphology is also seen in *Yarala burchfieldi* (see Muirhead & Filan 1995, pp. 132–133) and several Recent bandicoots (see Travouillon *et al.* 2010, character 18). In QM F53025, the posterior part of the p3 touches m1 and is slightly hidden by the anterior part of m1. However, in QM F52992 the

posterior cusp of p3 touches the anterior part of m1 but is not hidden as in QM F53025. In QM F52992, m1 is slightly shorter than p3, and the roots of m1 do not extend as far above the alveoli as do those of p3.

The morphology of m1 is as follows: the protoconid is the tallest cusp on the crown, followed (in decreasing order) by the metaconid, entoconid, paraconid, hypoconid and hypoconulid. The paraconid is large and positioned distinctly anterolingual to the protoconid, and anterior and slightly labial to the metaconid. The metaconid lies almost directly lingual to the protoconid, and hence the metacristid is perpendicular to the long axis of the tooth row. The paracristid is longer than the metacristid. In occlusal view, the hypoconid is more labially positioned than is the protoconid, i.e. the talonid is wider than the trigonid. The hypoconulid is low and positioned at the posterolingual tip of the crown, directly posterior to the entoconid. The posthypocristid connects the hypoconid to the hypconulid. The entoconid is the tallest cuspid on the talonid and is positioned on the lingual margin of the tooth, between the metaconid and hypoconulid. The entoconid is rounded on its posterior surface without a postentocristid in dental morphotype L2 (Fig. 6C, D), but an obliquely posterolabial oriented postentocristid is present in dental morphotype L1 (Fig. 6A, B). The anterior surface has a large, high pre-entocristid that terminates within the valley separating the entoconid and the metaconid. The trigonid basin is narrower than the talonid and opens on the lingual side between the para- and metaconids. The paracristid is the longest crest on the crown, followed (in decreasing length) by the: posthypocristid, cristid obliqua, metacristid, pre-entocristid and postentocristid (the latter two are approximately the same size). The anterior cingulid is large and visible in dental morphotype L1 (Fig. 6A, B), but absent in dental morphotype L2 (Fig. 6C, D) while a posterior cingulid is consistently absent in all specimens. The talonid basin is wide. The talonid basin is not open at any point, although the cristid obliqua is relatively low.

The morphology of m2 is similar to that of m1 except as follows. The trigonid is anteroposteriorly longer and labiolingually wider on m2. The anterior cingulum is also longer and wider, terminating at the anterolabial tip of the protoconid. The paraconid appears to be closer to the metaconid and hence the paracristid is more transverse across the tooth. The cristid obliqua terminates more lingually against the trigonid compared to m1, midway between the protoconid and metaconid. The metacristid is longer than on m1 and the metacristid notch is also positioned more lingually compared to m1. The hypoconid is positioned further labial than that on m1, and hence the talonid is wider. The angle between the cristid obliqua and the posthypocristid is smaller than in m1, and these two crests are also longer than on m1. The m2 as a whole is wider labiolingually than m1, but is approximately equal in anteroposterior length to m1.

The morphology of m3 is similar to m2 except as follows: the paraconid is positioned slightly closer to the metaconid, and hence the angle between the paracristid and metacristid is smaller. The protoconid extends labially to a greater degree than on m2, reaching almost as far as the hypoconid. The anterior cingulum is slightly wider (anteroposteriorly) than on m1 and m2. The trigonid and talonid are both labiolingually wider than on m1 and m2. The trigonid and talonid are not the same length (anteroposteriorly), with the talonid being longer.

The morphology of m4 is as for m3 except as follows. All cusps on the trigonid are smaller. The trigonid on m4 is approximately the same size as on m2. The protoconid is in a more lingual position than on m2 and m3, resulting in a slightly narrower trigonid than on m3. The talonid basin is reduced to a raised entoconid at its most posterolingual point and a smaller flatter hypoconid on the labial side in dental morphotype L1 (Fig. 6A, B), but the talonid is further reduced in dental morphotype L2, L3 and L4 (Fig. 6C–H). Measurements of the lower dentition of *B. palara* are presented in Online Supplementary Material Table 1.

Upper dentition. The description of the upper morphology is based largely based on QM F23440. Three cusps are present on P3, arranged anteroposteriorly. The anterior cusp is small. The major cusp is positioned centrally on the crown. The posterior cusp is larger than the anterior cusp but smaller than the major central cusp. The widest point of the tooth occurs between the central and posterior cusp. A distinct, sharp crest connects the major, central cusp to the posterior cusp, but there is no crest connecting the major cusp to the anterior cusp (see Fig. 7A, B).

The description of M1 here is based on QM F23435 because this tooth is better preserved in this specimen than in QM F23440. M1 is labiolingually narrower but anteroposteriorly slightly longer than both M2 and M3. Stylar cusp B lies directly labial to the paracone, and the preparacrista contacts stylar cusp B. A large stylar cusp C is present immediately posterior to stylar cusp B along the labial margin of the tooth. An additional, minute cusp is present immediately anterior to stylar cusp D along the labial margin of the tooth (St D1; see Turnbull *et al.* 2003, fig. 18.1). Stylar cusp B and C are connected by a crest, which continues posteriorly into the valley anterior to stylar cusp D1. This stylar cusp morphology resembles that of the M1 of cf. *Peroryctes tedfordi* from the Early Pliocene Hamilton Fauna in Victoria (see Turnbull *et al.* 2003, fig. 18.1). Stylar cusp D is a tall cusp positioned labial to the metacone. No crest extends anteriorly from stylar cusp D to D1. Stylar cusp E is present as a small cusp raised above the stylar crest connecting anteroposteriorly stylar cusp D to the metastyle (the posterolabial corner of the tooth). The protocone is low compared to this cusp on M2 and M3. The metaconule is very small and positioned lingual and

slightly anterior to the metacone. Stylar cusp D is the highest cusp on the crown (although it is broken on the M1 of QM F23435, see Fig. 7), followed (in decreasing height) by stylar cusp B, metacone, paracone, stylar cusp E, metastyle, stylar cusp C, stylar cusp D1, stylar cusp A, protocone and metaconule.

The postparacrista is slightly longer than the preparacrista, which is, in turn, longer than the anterior stylar crest (the crest that runs anteriorly–posteriorly from the anterior cingulum notch, through stylar cusp A to the anterior flank of stylar cusp B).

The premetacrista and postparacrista contact each other weakly forming a complete centrocrista, the apex of which lies very close to the valley between stylar cusp D1 and C. The preprotocrista terminates at the anterolingual base of the paracone and does not connect with the notched anterior cingulum tip; hence, the anterior cingulum is incomplete (see Travouillon *et al.* 2010, character 7). The postprotocrista connects the protocone to the metaconule, then continues through this cusp and terminates at the lingual base of the metacone and hence there is no posterior cingulum (see Travouillon *et al.* 2010, character 11). The angle between the preprotocrista and the postprotocrista at the protocone is wide, greater than 90°. The metastylar region is directed more labially than is the parastylar region due to the posterior edge of M1 touching the anterior edge of M2, while the parastylar region of M1 is more horizontal to the tooth row. The postmetacrista is the longest crest on the crown followed (in decreasing length) by premetacrista, preprotocrista, postprotocrista, postparacrista and preparacrista.

The morphology of M2 resembles that of M1 except as follows. The parastylar region is larger than in M1, and hence the paracone is in a more lingual position than on M1; the preparacrista and postparacrista are therefore also longer as a result. Stylar cusp A and stylar cusp B are taller than M1. The preparacrista extends labially to contact stylar cusp A. The protocone is further lingual than on M1, and the angle between the preprotocrista and postprotocrista is smaller, being approximately 90°. Stylar cusp D1 is present as a minute cusp, smaller than on M1. Stylar cusp E is reduced relative to M1.

The morphology of M3 resembles that of M2 except as follows. The paracone is in a more posterolingual position. The preparacrista and postparacrista are of approximately the same length, but the angle between these two crests is slightly smaller than on M2. Stylar cusp B is enlarged and slightly taller than stylar cusp D. Stylar cusp D1 is absent. Stylar cusp C is minute and is more lingually positioned than on M1 and M2. No posterior crest connects stylar cusp D to the metastyle. Stylar cusp E is also reduced in height compared to M2, and is rounded with no crest running through it. The metaconule is slightly wider than on M2. The angle between the postprotocrista and preprotocrista is less than 90°. The protocone is higher than on M2 and even more so than on M1. The postparacrista terminates at the point it meets with the premetacrista, at the anterior part of the base of stylar cusp D, forming a weak but complete centrocrista. The angle of the crests at the metacone is reduced so that the premetacrista runs directly towards stylar cusp D. The premetacrista contacts the base of stylar cusp D then curves anteriorly to join the postparacrista.

The morphology of M4 is well preserved in QM F23437 (the holotype; this tooth is slightly worn in this specimen) and QM F53586 (Fig. 7A) but this tooth is broken on QM F23435. The morphology of M4 resembles that of M3 except as follows: the parastylar region of M4 is significantly larger than on M1, M2 and M3. The metastylar region and metaconule are both absent on M4. The paracone is in a more posterolingual position, and stylar cusp B is approximately situated directly labial to the paracone as in the other teeth. The paracone is taller on M4 than M1–M3. The anterior cingulum and stylar cusp A are directly labial to the protocone. There is a small cusp posterior to stylar cusp B, which may be a reduced metacone or stylar cusp C or D. The preparacrista and postparacrista are longer than on M1, M2 and M3, with the preparacrista longer than the postparacrista (see Fig. 7A). The preparacrista connects to stylar cusp A and the postparacrista connects to the cusp posterior to stylar cusp B. The protocone is a distinct cusp that lies lingual and slightly anterior to the paracone (see Fig. 6). The preprotocrista and postprotocrista curve lingually, forming a v-shape, and join at the protocone. The height of the protocone is smaller than on M1–M3. No metaconule is present. Measurements of the upper dentition of *B. palara* are presented in Online Supplementary Material Table 2.

Variation within *Bulungu palara*

The large sample size of *Bulungu palara* exhibits considerable variation in molar morphology. We identify four distinct lower molar morphotypes (L1, L2, L3 and L4) and two distinct upper molar morphotypes (U1 and U2) in *B. palara*.

Morphotype L1 (as seen in QM F52992 from the FZB Camel Sputum Site; Fig. 6A, B) is characterized by the following features of m1–3: entoconid tall and distinct; pre-entocristid extends anteriorly and terminates at the base of the metaconid; entoconid with posterior crest (postentocristid) that fails to contact either hypoconulid or posthypocristid; angle between pre-entocristid and postentocristid approximately 90°. In addition, the talonid on m4 is narrower than in other lower molar morphotypes. This lower molar morphotype is the most common among *B. palara* specimens from Camel Sputum Site and from Riversleigh sites as a whole (Online Supplementary Material Table 1), and we tentatively match it to upper molar morphotype U1, which is present in the holotype skull (QM F23437) and is

the most common upper molar morphology found at Camel Sputum site and other Riversleigh sites.

Morphotype L2 (as seen in QM F24289 from the FZB Dirk's Tower Site; Fig. 6C, D) is characterized by the following features of m1–3: entoconid tall and distinct; pre-entocristid connects entoconid to posterior flank of metaconid; postentocristid absent (this crest is present in morphotypes L1 and L3); posthypocristid connects directly to hypoconulid.

Morphotype L3 (as seen in QM F52990 from the FZC Wang Site; Fig. 6E, F) is characterized by the following features of m3: entoconid tall and distinct; pre-entocristid and postentocristid both present, with the postentocristid not connecting to hypoconulid but instead connecting to posthypocristid at base of entoconid. The angle between pre-entocristid and postentocristid is approximately 100°, i.e. larger than in L1.

Morphotype L4 (as seen in QM F53002 from the FZC Gag Site; Fig. 6G, H) is characterized by the following features of m2–3: entoconid distinctly reduced compared to other morphotypes; entoconid connects anteriorly via pre-entocristid to base of metaconid; postentocristid absent.

These four different morphotypes may be temporally related, representing two different anagenetic lineages. Morphotype L1 may be ancestral to morphotype L3: both L1 and L3 exhibit a postentocristid (whereas this crest is absent both L2 and L4), but L3 exhibits an apparently more derived morphology in which the postentocristid connects to the posthypocristid, and L1 is present only in Riversleigh FZB sites, whereas L3 is present only in Riversleigh FZC sites (Online Supplementary Material Table 1). Similarly, morphotype L2 may be ancestral to morphotype L4: L4 appears more derived in having a distinctly reduced entoconid, and L2 is present in Riversleigh FZA and FZB sites whereas L4 is present only in Riversleigh FZC sites (Online Supplementary Material Table 1). Alternatively, these four lower molar morphotypes could in fact represent four different species of *Bulungu*, with two species present contemporaneously in Riversleigh FZB (L1 and L2) and two in Riversleigh FZC (L3 and L4). They are quite distinctively different and there is morphological change over time possibly representing two separate lineages (a lineage that includes L1 and L3 where the entoconid increases in size and the postentocristid extends to connect with the posthypocristid, and another that includes L2 and L4 where the entoconid reduces in size). SAM P66837 from the Kutjamarpu LF is too worn to confidently identify to a specific morphotype: it appears to represent either L1 or L4 (Online Supplementary Material Table 1).

Two distinct upper molar morphotypes, referred to here as U1 and U2, are also observed within *B. palara*. These two morphotypes are largely similar, but exhibit a number of distinguishing features.

Morphotype U1 (as seen in the holotype QM F23437 and also QM F53586, both from the FZB Upper Site; Fig. 7A) has the following characteristics: (1) stylar cusp B larger than stylar cusp C on M1; (2) the crest joining stylar cusp B to C on M1 is parallel to the tooth row; (3) the preparacrista of M2 connects to stylar cusp A; (4) the metaconule on M3 is larger than in U2 and is more lingually positioned; (5) M4 is longer anteroposteriorly in U1 than in U2; and (6) stylar cusp B is identifiable on M4 as a distinct cusp.

Morphotype U2 (as seen in QM F52993 from the FZB Camel Sputum Site; Fig. 7B) has the following characteristics: (1) stylar cusp C larger than stylar cusp B on M1; (2) the crest joining stylar cusp B to C on M1 is parallel to the postparacrista; (3) the preparacrista of M2 connects to stylar cusp B; (4) the metaconule on M3 is smaller than in U1 and more labially positioned; (5) M4 is wider labiolingually in U2 than in U1; and (6) stylar cusp B is absent on M4. Unlike the lower molar morphotypes, there does not seem to be a clear relationship between the upper molar morphotypes and the Riversleigh Faunal Zones: U1 is known from FZA, FZB and FZC, whereas the rarer U2 morphotype (which we observed in only three specimens) is present in FZB only (Online Supplementary Material Table 2). SAM P108072 from the Kutjamarpu LF exhibits the U1 morphotype.

Results

Phylogenetic analyses

In all four phylogenetic analyses presented here, i.e. unconstrained maximum parsimony, maximum parsimony with a molecular scaffold (Fig. 9), unconstrained Bayesian analysis and Bayesian analysis with a molecular scaffold (Fig. 10), *Bulungu palara* is recovered outside crown-group Peramelemorphia. The other Oligo-Miocene peramelemorphians included here, namely *Galadi speciosus* from Riversleigh FZA and FZB, *Yarala burchfieldi* from Riversleigh FZB and FZC and *Yarala kida* from the Late Oligocene Kangaroo Well Local Fauna, are also placed outside crown-group Peramelemorphia. However, relationships between the four Oligo-Miocene peramelemorphians are unstable: unconstrained maximum parsimony (Fig. 9A) placed all four in a clade, but with weak support (bootstrap = <50%; decay index = +1); maximum parsimony with a molecular scaffold (Fig. 9B) placed *Bulungu* as the sister taxon of the crown-group + *Ischnodon*, with *Galadi* and *Yarala burchfieldi* + *Y. kida* successively more distant; neither the unconstrained Bayesian analysis (Fig. 10A) nor Bayesian analysis with a molecular scaffold (Fig. 10B) resolved the relationships of *Bulungu*, *Galadi* or *Yarala* beyond placing them outside the crown-group.

Support for the monophyly of crown-group Peramelemorphia to the exclusion of *Bulungu*, *Galadi* and *Yarala* was weak in the unconstrained maximum parsimony analysis (bootstrap = <50%; decay index = +1), but stronger in the unconstrained Bayesian analysis (Bayesian posterior probability = 0.91). Within the crown group,

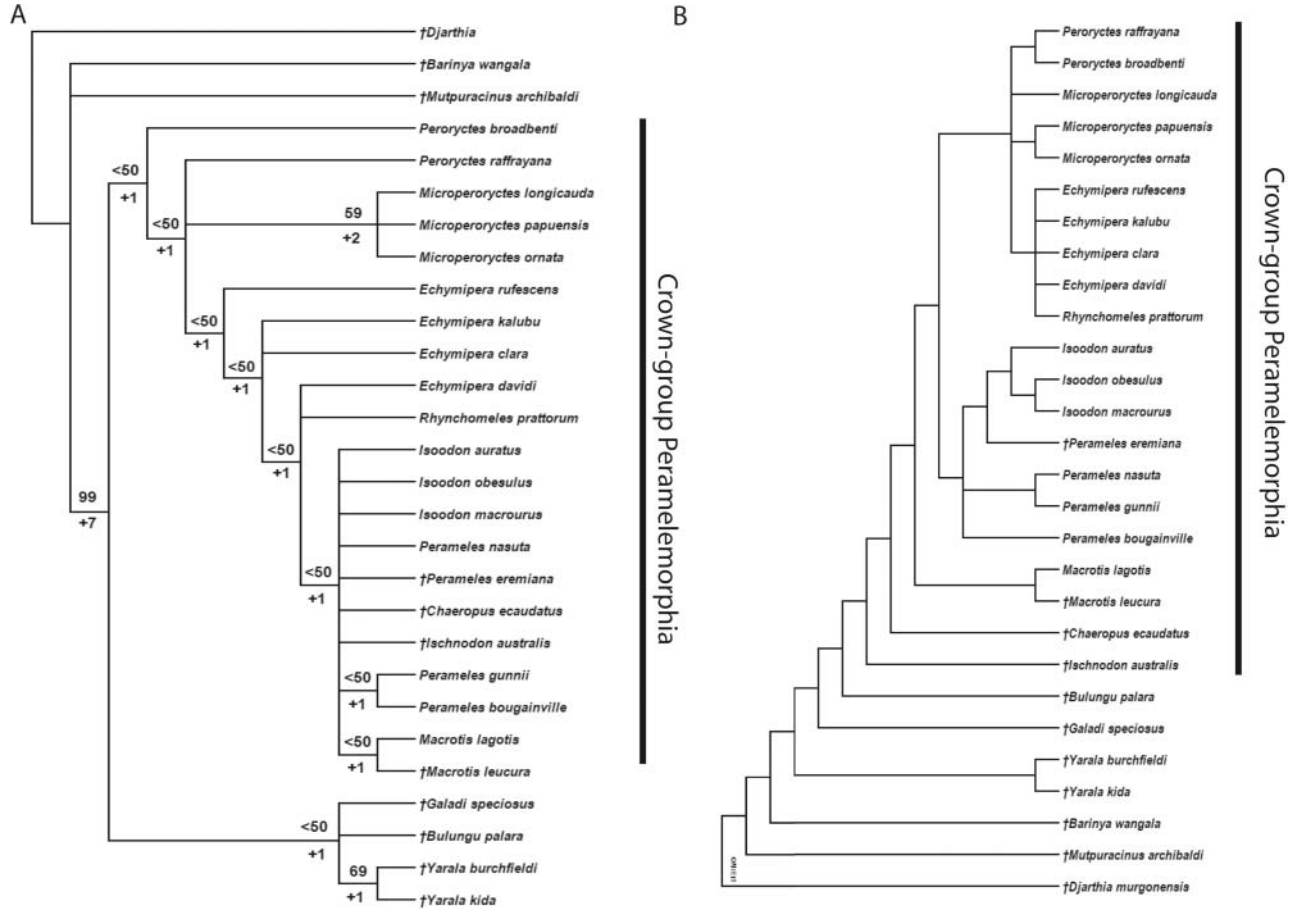

Figure 9. Phylogenetic relationships of *Bulungu palara* gen. et sp. nov. based on maximum parsimony analysis of a 74 character craniodental matrix. Fossil and recently extinct taxa are indicated by †. Crown-group Peramelemorphia is indicated. **A,** strict consensus of 78 most parsimonious trees (tree length = 322; consistency index excluding uninformative characters = 0.4044; retention index = 0.6828) from unconstrained maximum parsimony analysis of the matrix; numbers above branches represent bootstrap values (250 replicates); numbers below branches represent decay indices. **B,** strict consensus of 15 most parsimonious trees (tree length = 350; consistency index excluding uninformative characters = 0.3718; retention index = 0.6361) that result when the matrix is analysed using maximum parsimony and enforcing a 'backbone' molecular scaffold based on Westerman *et al.* (2012).

the unconstrained analyses are incongruent with recent molecular phylogenies (e.g. Westerman *et al.* 2001, 2012; Meredith *et al.* 2008) in failing to support monophyly of Peroryctidae (i.e. *Echymipera* + *Microperoryctes* + *Peroryctes* + *Rhynchomeles*) and in placing *Macrotis* and *Chaeropus* in a clade with the peramelids *Perameles* and *Isoodon*, rather than outside Peroryctidae + Peramelidae.

The Pliocene *Ischnodon* is placed in a clade with *Macrotis*, *Chaeropus*, *Perameles* and *Isoodon* in both the unconstrained maximum parsimony and unconstrained Bayesian analyses, although support for this clade is strong in the latter analysis only (Bayesian posterior probability = 1.00), and relationships within this clade are largely unresolved. By contrast, the maximum parsimony molecular scaffold analysis recovers *Ischnodon* as the sister taxon to crown-group Peramelemorphia, while the Bayesian molecular scaffold analysis places *Ischnodon* at the base of the crown group. Strikingly, *Ischnodon* does not form a clade with the thylacomyids *Macrotis lagotis* and *M. leucura* in any of our analyses (*contra* Stirton 1955), nor does it appear to be particularly closely related to any other Recent peramelemorphian genus.

Morphotype analysis

Fig. 11 shows the plots of the upper premolar and molar length versus width for *Bulungu palara*, *Yarala burchfieldi* and Genus 3 sp. 1. There is no overlap in upper premolar dimensions between the three species. However, there is no clear separation in terms of premolar dimensions between the two morphotypes (U1 and U2) of *B. palara*. Similarly, *B. palara* morphotypes U1 and U2 show very little difference in molar dimensions, overlapping each other without forming any clearly distinct groups.

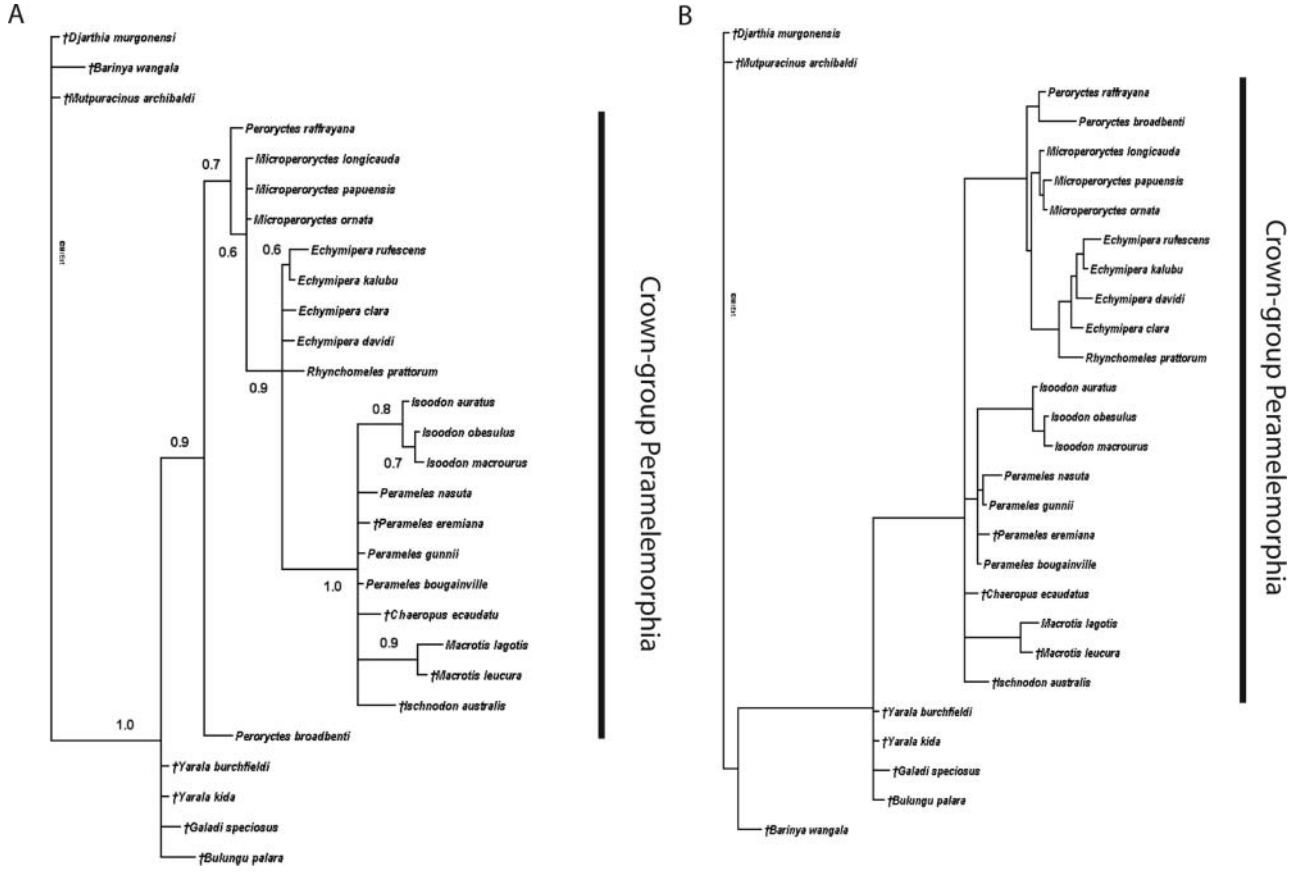

Figure 10. Phylogenetic relationships of *Bulungu palara* gen. et sp. nov. based on Bayesian analysis of a 74 character craniodental matrix. Fossil and recently extinct taxa are indicated by †. Crown-group Peramelemorphia is indicated. Numbers above branches represent Bayesian posterior probabilities. **A,** 50% majority rule consensus that results after unconstrained Bayesian analysis of the matrix assuming the Mk + G model (harmonic mean of the log likelihood of the post-burn-in trees = −1020.96); the analysis was run for two million generations, sampling trees every 1000 generations, with a burn-in period of one million generations. **B,** 50% majority rule consensus that results after Bayesian analysis of the matrix assuming the Mk + G model and enforcing a 'backbone' molecular scaffold based on Westerman *et al.* (2012; harmonic mean of the log likelihood of the post-burn-in trees = −1789.26) the analysis was run for five million generations, sampling trees every 1000 generations, with a burn-in period of four million generations. Branch lengths are proportional to the number of character state changes.

However, upper molar dimensions of larger specimens of *Y. burchfieldi* overlap with those of smaller specimens of *B. palara*, suggesting that isolated specimens cannot be assigned to either species based on size alone. Interestingly, specimens of *Y. burchfieldi* tend to be larger (mainly as a result of increased length) in Faunal Zone C than B.

In the lower dentition (Fig. 12), premolar dimensions show a similar pattern as seen in the upper premolars, namely no overlap between *Bulungu palara*, *Yarala burchfieldi* and Genus 3 sp. 1. However, Genus 3 sp. 1 shows a remarkable increase in third premolar size in Faunal Zone C compared to B, and Genus 5 sp. 1 seems to overlap in size with *Y. burchfieldi.* No distinct separation in terms of premolar dimensions is observed between the four morphotypes of *B. palara*, although the third premolar of morphotype L2 seems to be slightly longer and wider than morphotype L1. In the lower molars, specimens of *Y. burchfieldi* and Genus 3 sp. 1 from Faunal Zone C are typically larger than Faunal Zone B. Genus 5 sp. 1 again appears to overlap in size with *Y. burchfieldi*, whereas specimens of Genus 5 sp. 2 overlap in terms of length with *B. palara*, but not in terms of width. Molar size of the four lower morphotypes of *B. palara* show considerable overlap, but as for the premolars, morphotype L2 seems to be slightly longer and wider than morphotype L1. There do not seem to be any trends between the size of specimens of Faunal Zone B and C.

Calculated univariate statistics, including coefficients of variation, are shown in Online Supplementary Material Table 3; these results are calculated from the measurements of upper (Online Supplementary Material Table 4) and lower (Online Supplementary Material Table 5) dentition of extant bandicoots. Coefficient of variation of dental dimensions for *Bulungu palara* generally fall within expected levels (4–10; Simpson *et al.* 1960) for a single, mixed-

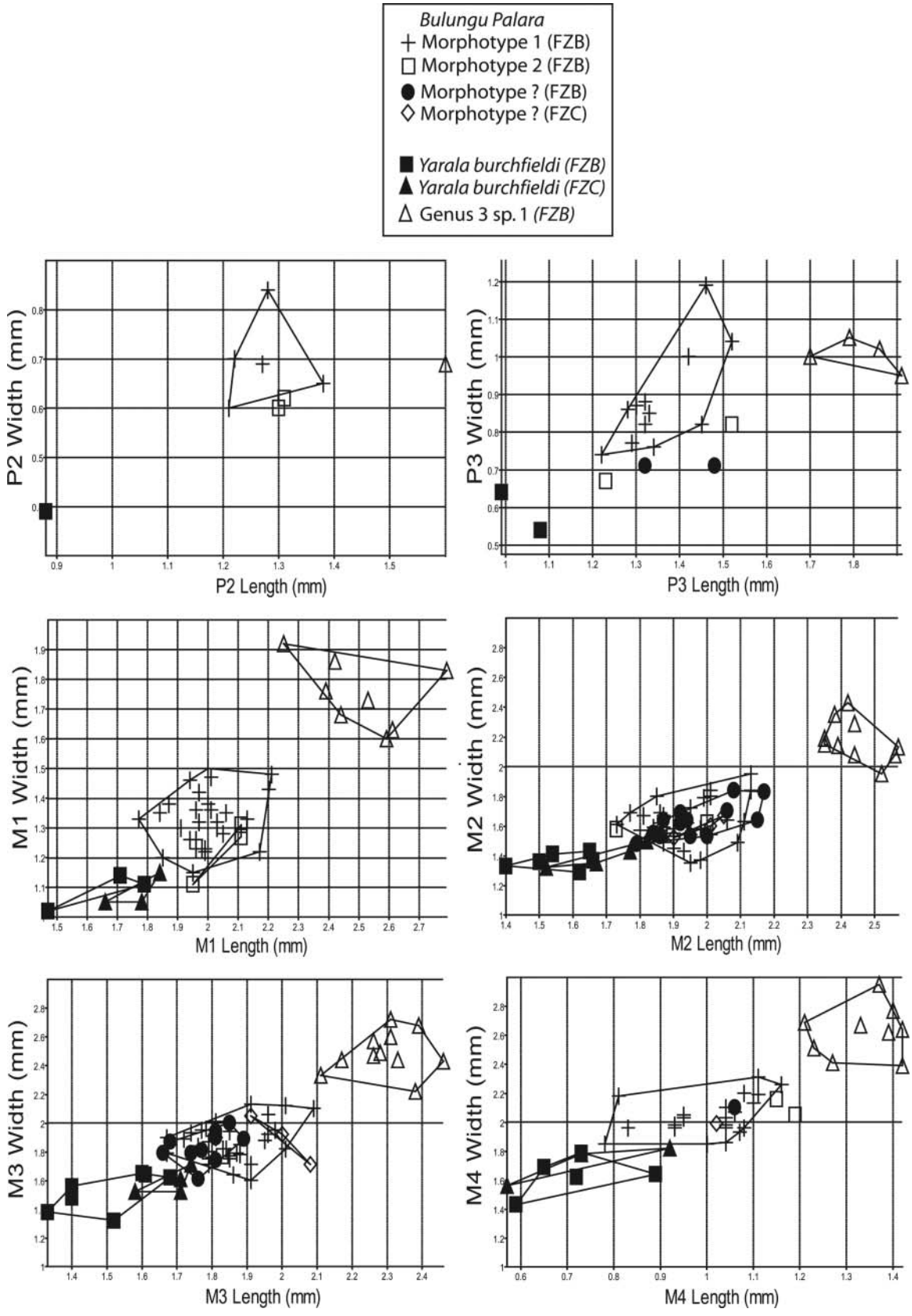

Figure 11. Morphotype plot of length versus width in millimetres of upper premolars and molars. Comparisons of morphotypes of *Bulungu palara* with *Yarala burchfieldi* and other undescribed fossil bandicoot species.

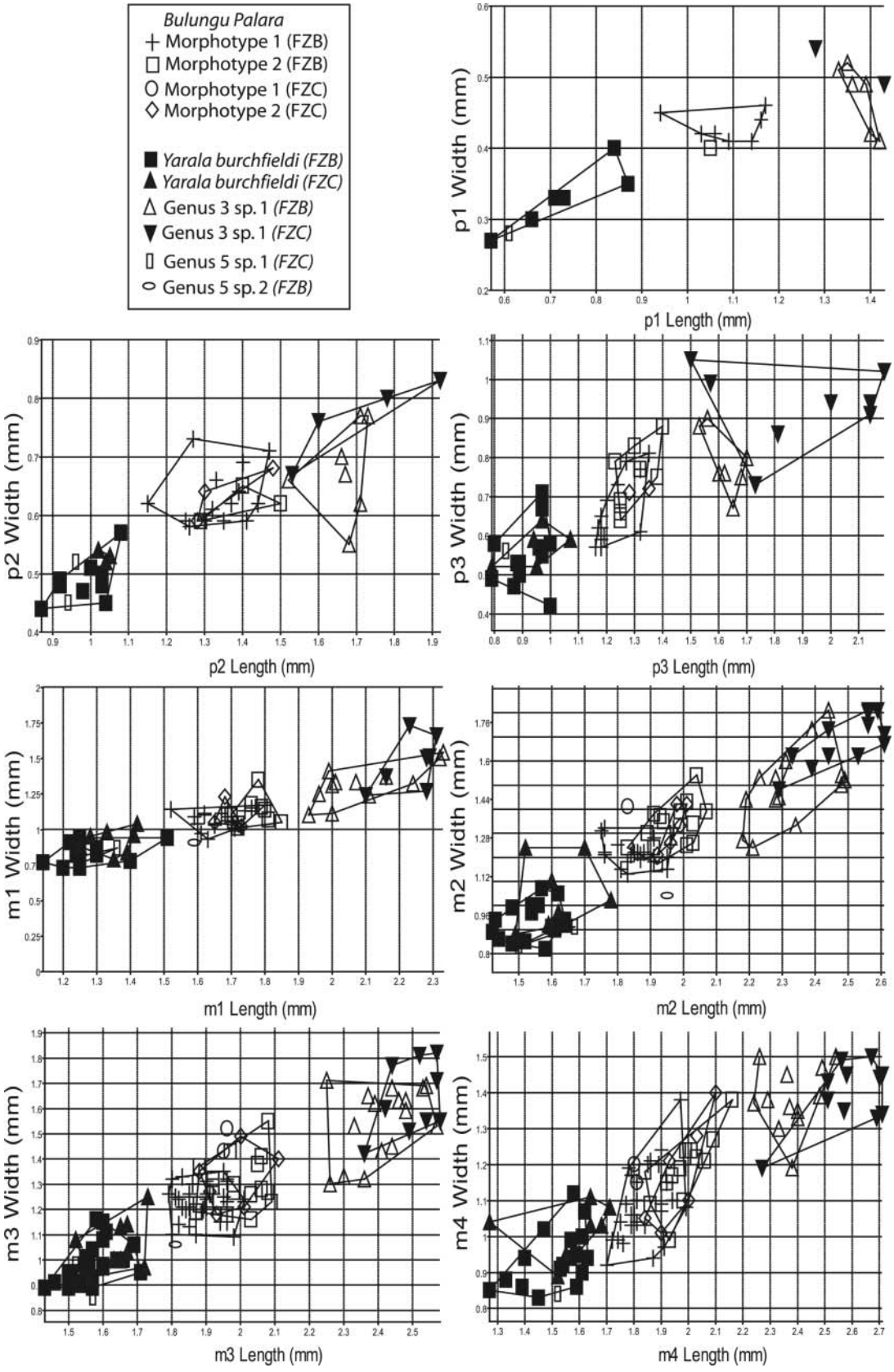

Figure 12. Morphotype plot of length versus width in millimetres of lower premolars and molars. Comparisons of morphotypes of *Bulungu palara* with *Yarala burchfieldi* and other undescribed fossil bandicoot species.

sex, normally-distributed population (Online Supplementary Material Table 3), except for p3 (CV = 12.79) and P3 (CV = 15.73) width and M4 (CV = 11.67) length. This is consistent with results from modern bandicoot species, where coefficients of variation for p3, P3 and M4 are also in many cases higher than 10. This finding is perhaps not surprising, as considerable variation in third premolar size (some of which is sexually dimorphic) has been documented in several modern bandicoot species (Aplin *et al.* 2010), and M4 is generally the morphologically most variable molar in marsupials because it is not constrained by the need to occlude with a more posterior lower molar.

The variation present in the specimens described here led Muirhead (1994) to initially recognize multiple species of *Bulungu*, but subsequently she placed them in a single species. We agree with the latter decision; based on our analyses of dental variation among fossil and modern bandicoot species, we consider that the morphological variation encompassed by the specimens referred here to *B. palara* does not warrant recognition of more than a single species, at least until further fossil material is found that might provide additional, compelling evidence in favour of splitting this species.

Discussion

Phylogeny

Despite the increased sampling of taxa (both fossil and extant) and characters in our morphological matrix compared to that used by Travouillon *et al.* (2010), our phylogenetic results are not particularly stable across the different analyses presented here. In particular, support values are low (bootstrap <50%; decay index = +1) for most nodes within Peramelemorphia in our unconstrained maximum parsimony analysis; however, this is perhaps to be expected, as adding more fossil taxa has been shown to result in lower support values in general (Cobbett *et al.* 2007). Support values in our unconstrained Bayesian analysis are generally higher, but Bayesian posterior probabilities have been shown to overestimate support if an inappropriate model is used (e.g. Erixon *et al.* 2003). Also of note is the conflict between our unconstrained maximum parsimony and Bayesian analyses and recent molecular phylogenies (e.g. Westerman *et al.* 2001, 2012; Meredith *et al.* 2008): our unconstrained analyses fail to support monophyly of Peroryctinae + Echymiperinae, and place *Macrotis* and *Chaeropus* in a clade with the perameline genera *Isoodon* and *Perameles*, rather than outside Peroryctinae + Echymiperinae + Peramelinae.

Despite this instability and conflict with molecular data, it is noteworthy that *Bulungu* falls outside crown-group Peramelemorphia in all four analyses presented here (including when a molecular scaffold is used), as do the other Oligo-Miocene peramelemorphians included in our matrix, namely *Galadi speciosus*, *Yarala burchfieldi* and *Y. kida*. Monophyly of crown-group Peramelemorphia to the exclusion of these Oligo-Miocene forms is weakly supported in the unconstrained maximum parsimony analysis (bootstrap < 50%; decay index = +1) but more strongly supported in the unconstrained Bayesian analysis (Bayesian posterior probability = 0.91). We note that the three Oligo-Miocene forms known from cranial remains, namely *Bulungu palara*, *Galadi speciosus* and *Yarala burchfieldi*, are characterized by: (1) a premaxilla that is taller than it is long, with a maxilla–nasal contact longer than the premaxilla–nasal contact (character 30–0); (2) nasals that extend posteriorly past the anterior rim of the orbit (character 32–0); and (3) alisphenoid–parietal (rather than squamosal–frontal) contact (character 38–0); based on comparison with relevant outgroup taxa that are known from cranial material (i.e. dasyuromorphians), these character states appear to be plesiomorphic within Peramelemorphia and are not seen in any known crown-peramelemorphian. We are therefore relatively confident that *Bulungu*, *Galadi* and *Yarala* are stem- rather than crown-peramelemorphians. However, our analyses fail to consistently resolve the precise relationships of *Bulungu*, *Galadi* and *Yarala*, beyond placing them outside crown-group Peramelemorphia; it is unclear from our results whether they represent a paraphyletic grade of stem-forms (as suggested by Travouillon *et al.* 2010), or, alternatively, an extinct clade. We therefore suggest that *Bulungu*, *Galadi* and *Yarala* be referred to Peramelemorphia *incertae sedis* pending further studies that might clarify their relationships. By contrast, Muirhead (2000) placed *Yarala* in its own family, Yaralidae, and superfamily, Yaraloidea; however, Muirhead's (2000) diagnoses of Yaralidae and Yaraloidea are problematic because they are based purely on craniodental features that appear to be plesiomorphic for Peramelemorphia as a whole. As a result, it is highly unlikely that Yaralidae and Yaraloidea *sensu* Muirhead (2000) represent monophyletic groups (but rather paraphyletic grades of stem-peramelemorphians), and hence we do not recommend their use pending further phylogenetic studies that might substantiate their monophyly.

The Pliocene peramelemorphian *Ischnodon australis* was described as a thylacomyid by Stirton (1955), and this identification has been endorsed in subsequent publications (e.g. Archer & Bartholomai 1978). However, the proposed relationship between *Ischnodon* and the Recent thylacomyids *Macrotis lagotis* and *M. leucura* has never been tested by formal phylogenetic analysis before now. None of our four analyses support an *Ischnodon* + *Macrotis* clade, nor an exclusive relationship between *Ischnodon* and any other Recent peramelemorphian genus; we argue, therefore, that *Ischnodon* should not be considered as the earliest record of Thylacomyidae (*contra* Stirton 1955; Archer & Bartholomai 1978). However, *Ischnodon* appears to be

more closely related to crown-group Peramelemorphia than are the Oligo-Miocene forms *Bulungu*, *Galadi* and *Yarala*, and falls within the crown group in three of the four analyses (with the exception of the maximum parsimony with molecular scaffold analysis).

Although Westerman *et al.* (2012) argued, based on molecular divergence dates calculated using a 'relaxed molecular clock', that early members of crown-group Peramelemorphia should be expected to be present in Australian Oligo-Miocene fossil sites, these have yet to be identified; as noted above, we are relatively confident that *Bulungu*, *Yarala* and *Galadi* are not crown-group forms. In addition, it is unclear whether the Pliocene *Ischnodon* is a crown-peramelemorphian or not; certainly, it does not appear to be a thylacomyid. *Perameles bowensis* from the Bow Local Fauna (note that Turnbull *et al.* 2003 suggested that material referred to *P. bowensis* by Muirhead *et al.* 1997 may represent multiple taxa), *P. allinghamensis* from the Bluff Downs Local Fauna, and two forms from the Hamilton Local Fauna referred to cf. *Peroryctes* by Turnbull *et al.* (2003) are all Early Pliocene in age and collectively may represent the oldest known crown-peramelemorphians, but their relationships have yet to be tested by formal phylogenetic analysis, and so their membership of the crown group remains tentative.

The apparent discrepancy between the fossil record of crown-group Peramelemorphia (the oldest members of which are questionably early Pliocene) and the molecular divergence dates calculated by Westerman *et al.* (2012) may be due to inadequate fossil sampling, misidentification of fossil taxa and their phylogenetic relationships (which may be an issue given the conflict between our unconstrained morphological analyses and recent molecular phylogenies), or a combination of the two. Alternatively, it may be the result of problems with the molecular dating approach employed by Westerman *et al.* (2012), as recent studies have suggested that the rate of molecular evolution may undergo sudden shifts that cannot be accounted for by many currently used molecular dating methods (Kitazoe *et al.* 2007; Waddell 2008; Dornburg *et al.* 2012), including the uncorrelated lognormal relaxed clock model used by Westerman *et al.* (2012; see Dornburg *et al.* 2012); if so, it is possible that the divergence dates presented by Westerman *et al.* (2012) are overestimates, and that the deep divergences of crown-group Peramelemorphia largely post-date the Late Oligocene–Early Miocene.

Progress towards reconciling the fossil-based and molecular estimates of peramelemorphian phylogeny and divergence times is likely to be achieved via a number of avenues. Addition of morphological characters from other anatomical systems besides the cranium and dentition (e.g. the postcranial skeleton, external morphology) may help improve resolution and reduce conflict with recent molecular phylogenies. Inclusion of additional fossil peramelemorphians – for example, undescribed taxa from Oligo-Miocene deposits in Riversleigh, and the Pliocene forms *Perameles bowensis*, *P. allinghamensis* and cf. *Peroryctes tedfordi* – may also be of use, particularly in clarifying the time of origin of the crown group. However, many of these fossil taxa (notably the Pliocene forms discussed) are known from highly fragmentary dental remains, and so it may not be possible to robustly resolve their relationships based on available material. Improvements in the peramelemorphian fossil record, with the discovery of new, well-preserved cranial and post-cranial material, would seem to offer the best hope of improving our understanding of bandicoot evolution; however, such material is currently known only from Riversleigh, and much of it remains to be described.

Palaeoecology of *Bulungu palara* and convergence with dasyurids

Based on available data, Recent bandicoots and bilbies appear to be generally omnivorous, with smaller species somewhat more insectivorous. By contrast, the very small size (skull length ~30 mm; average estimated body mass of ~65 g) and dental morphology (e.g. the presence of a complete centrocrista that is not highly invasive of the stylar region, and a vestigial metaconule) of *Yarala burchfieldi* suggest a primarily or exclusively insectivorous diet, while *Galadi speciosus* was a large (~900 g) brevirostral form with powerful temporalis musculature, and probably filled a more carnivorous niche (see Travouillon *et al.* 2010).

With a skull length of ~33 mm and an average estimated body mass of 131 g (see Travouillon *et al.* 2009, Genus 1 sp. 1), the new taxon described here, *Bulungu palara*, is one of the smallest bandicoots (including as yet undescribed forms) collected from the Riversleigh deposits to date, larger only than *Yarala burchfieldi*. The estimated body mass of *Bulungu palara* is much smaller than that of any modern Australian bandicoot (Strahan 1995), which range in size from 226 g (the western barred bandicoot, *Perameles bougainville*) to 2500 g (the greater bilby, *Macrotis lagotis*). Modern New Guinean bandicoots exhibit a much wider range of sizes, although detailed body mass estimates are unavailable. However, we note that the smallest known extant bandicoot, *Microperoryctes aplini* (the Arfak pygmy bandicoot), which is endemic to the Arfak mountains in the Vogelkop Peninsula of Papua Province (Indonesia), has a skull length of approximately 42–43 mm (Helgen & Flannery 2004), whereas skull length for *Y. burchfieldi* is approximately 30 mm, and that of *B. palara* is approximately 33 mm. Given that skull length is a good predictor of body mass in marsupials (Myers 2001), it seems highly likely that both *Y. burchfieldi* and *B. palara* would both have weighed considerably less than *M. aplini*.

Based on the proportions of available cranial material and isolated dentaries (specifically the absence or small

size of diastemata in the lower dentition), both *Yarala* and *Bulungu* are also characterized by relatively short snouts compared to modern bandicoots, although probably not to the extreme seen in *Galadi*. The precise ecological significance of rostral shape in modern and fossil bandicoots remains unclear pending quantitative functional analyses, but we note that it correlates strongly with diet in marsupials: specifically, a shorter snout indicates higher relative bite force and larger relative prey size (Wroe & Milne 2007).

Given its small size and cranial shape, we suspect that *B. palara* was (like *Y. burchfieldi*) probably more insectivorous than modern bandicoots for which dietary information is available (unfortunately, we are unaware of data concerning the diet of the extant species *Microperoryctes aplini* and *M. murina*). However, *B. palara* is characterized by a better-developed metaconule and more invasive centrocrista than *Y. burchfieldi*; these dental features imply a greater degree of transverse jaw movement in *B. palara*, potentially indicative of a more omnivorous diet. This, together with its larger size (~131 g compared to 65 g), suggests that *B. palara* was probably somewhat more omnivorous than *Y. burchfieldi*. *Yarala* and *Bulungu* may both have occupied a very different niche to extant bandicoots, perhaps a similar niche that is now occupied by small insectivorous dasyurids such as *Antechinus godmani* (95 g males, 58 g females) (Strahan 1995) in Australia or *Murexechinus melanurus* in New Guinea (skull length 26–27 mm; Van Dyck 2002).

Interestingly, *B. palara* shares some dental features with a fossil ?dasyurid, *Wakamatha tasselli* (Archer & Rich 1979) from Billeroo Creek, which is possibly part of the Namba Formation (Late Oligocene to Early Miocene in age) or, alternatively, the Pleistocene Eurinilla Formation. The entoconid of *Wakamatha tasselli* is crescent-shaped, as is the entoconid of *B. palara* morphotypes L1 and L3. Archer & Rich (1979) noted that this feature was also present in the modern dasyurid *Sminthopsis crassicaudata*, and suggested an adaptation enabling greater transverse jaw movement and finer commutation of foods. Future studies will involve the use of dental microwear and finite element analysis to investigate the probable diet and palaeoecology of *Bulungu palara* and the other Riversleigh fossil bandicoots.

Biocorrelative potential of *B. palara*

As observed by Schwartz (2006), bandicoots are relatively common in Australian Cenozoic fossil localities and hence have considerable potential for biocorrelation of Australian fossil faunas, most of which still lack absolute dates. However, this promise has yet to be fulfilled, as much of this bandicoot material remains undescribed and the species-level taxonomy and phylogeny of Peramelemorphia remains to be confidently resolved. In contrast to most Australian fossil sites, fossil bandicoots from Riversleigh are represented by abundant, well-preserved material, including relatively complete cranial specimens and associated postcranial elements, rather than purely isolated dental specimens. Thus, study of the Riversleigh bandicoots is likely to be key to unlocking the biocorrelative potential of the group as a whole. However, the presence of the new Riversleigh bandicoot described here, *Bulungu palara*, in another Australian fossil fauna, namely the Kutjamarpu Local Fauna in the Lake Eyre Basin of South Australia (see Fig. 8A–D), is congruent with current estimates of the ages of these faunas, namely Late Oligocene–Middle Miocene for Riversleigh Faunal Zones A–C and Early–Middle Miocene for the Kutjamarpu LF. As discussed above, the occurrence of lower molar morphotypes of *B. palara* in Riversleigh sites appears to be related to the Riversleigh Faunal Zones: morphotype L2 occurs in FZA and FZB, L1 occurs only in FZB and L3 and L4 occur only in FZC. Assuming that FZC is indeed younger (Middle Miocene) than FZA (Late Oligocene) and FZB (Early Miocene), then this distribution appears to be temporally related; this raises the possibility that the different *B. palara* lower molar morphotypes might allow finer-scaled biocorrelation between Australian fossil sites than does simply presence or absence of the species as a whole. Frustratingly, however, the only *B. palara* specimen from the Kutjamarpu LF that preserves the lower molars, SAM P66837, is worn, and it is unclear whether it represents morphotype L1 or L4; if it is L1, then this would suggest that the Kutjamarpu LF is similar in age to Riversleigh FZB (Early Miocene), whereas if it is L4, this would imply a similar age to Riversleigh FZC (Middle Miocene). Collection of additional, less worn *B. palara* specimens from the Kutjamarpu LF might help resolve this issue, and test Black *et al.*'s (2012) hypothesis that the Kutjamarpu LF is intermediate in age between FZB and FZC, which was based on stage-of-evolution biocorrelation using the diprotodontid genus *Neohelos*.

Ongoing work suggests that other undescribed bandicoot taxa from Riversleigh are also present in the Kutjamarpu Local Fauna, and that close relatives of these taxa are present in the Ditjimanka and Ngapakaldi Local Faunas of the Lake Eyre Basin, and possibly other localities such as Kangaroo Well and Bullock Creek Local Faunas in the Northern Territory. Study of these taxa is likely to lead to further refinement and revision of our current understanding of the relative and absolute ages of Australian Cenozoic fossil faunas (see e.g. Megirian *et al.* 2010).

Conclusions

Bulungu palara represents the third fossil bandicoot to be described from Oligo-Miocene deposits at Riversleigh World Heritage Property, north-western Queensland, and only the fourth to be described from pre-Pliocene sites in Australia. Based on its craniodental morphology, *B. palara* appears to lie outside crown-group Peramelemorphia, as do the three other Oligo-Miocene bandicoots described to date, namely *Yarala burchfieldi*, *Y. kida* and *Galadi speciosus*; although dated molecular phylogenies suggest that crown-group bandicoots should be present in Oligo-Miocene

deposits, these have yet to be found. The presence of *B. palara* in the Kutjamarpu Local Fauna of South Australia is congruent with current estimates for the ages of Riversleigh Faunal Zones A–C (Late Oligocene–Middle Miocene) and the Kutjamarpu Local Fauna (Early–Middle Miocene), and hints at the potential of bandicoots for biocorrelation of Australian fossil sites. Our identification and description of distinct, potentially temporally related dental morphotypes within *B. palara* should allow finer-scale biocorrelation than indicated by simple presence or absence of the species. The small size (~130 g) and craniodental morphology of *Bulungu palara* suggest that it was more insectivorous than modern bandicoots. Together with the very small (~65 g), probably insectivorous *Yarala burchfieldi* and large (~900 g), probably predominantly faunivorous *Galadi speciosus* (see Travouillon *et al.* 2010), *B. palara* suggests that Oligo-Miocene Australian bandicoots occupied ecological niches that today are predominantly filled by members of another marsupial clade, namely Dasyuridae.

Acknowledgements

Support for research at Riversleigh has come from the Australian Research Council (DP0453262, LP0453664 & LP0989969 grants to Mike Archer and Sue Hand at the University of New South Wales); XSTRATA Community Partnership Program (North Queensland); the University of New South Wales; the Queensland National Parks and Wildlife Service; Environment Australia; the Queensland Museum; the Australian Museum; the Riversleigh Society, Inc.; Outback at Isa; Mount Isa City Council; and private supporters including Elaine Clark, Margaret Beavis, Martin Dickson, Sue and Jim Lavarack, and Sue and Don Scott-Orr. Yamila Gurovich's research was partially funded by CONICET (Beca Postdoctoral Extraordinaria), and Robin Beck's research was funded by NSF grant DEB-0743039 (in collaboration with Robert Voss at AMNH). Assistance in the field has come from many hundreds of volunteers as well as staff and postgraduate students of the University of New South Wales. Mike Lee (South Australian Museum and University of Adelaide) provided assistance with MrBayes. Many thanks to Suzanne Hand, Karen Black, Anna Gillespie, Henk Godthelp, Jackie Nguyen, Vera Weisbecker and Trevor Worthy for their help, support and feedback, as well as Sandy Ingleby and Anja Divljan (Aust Museum) for providing access to modern Peramelemorphia.

Supplementary material

Supplementary material is available online DOI: 10.1080/14772019.2013.776646
The matrix is available for download from morphobank.org, project number 758.

References

Aplin, K. P. 1990. *Basicranial regions of diprotodontian marsupials: anatomy, ontogeny and phylogeny*. Unpublished PhD thesis, University of New South Wales, 389 pp.

Aplin, K. P. & **Archer, M.** 1987. Recent advances in marsupial systematics with a new syncretic classification. Pp. xv–lxxii in M. Archer (ed.) *Possums and Opossums, Studies in Evolution*. Surrey Beatty & Sons, and the Royal Zoological Society of New South Wales, Sydney.

Aplin, K. P., **Helgen, K. M.** & **Lunde, D.** 2010. Review of the morphology, distribution and conservation status of *Peroryctes broadbenti* (Ramsay, 1879), the giant bandicoot of south-eastern Papua New Guinea. *American Museum Novitates*, **3696**, 1–41.

Archer, M. 1976. The dasyurid dentition and its relationships to that of didelphids, thylacinids and borhyaenids. *Australian Journal of Zoology*, Supplementary Series **39**, 1–34.

Archer, M. & **Bartholomai, A.** 1978. Tertiary mammals of Australia: a synoptic review. *Alcheringa*, **2**, 1–19.

Archer, M. & **Rich, T.** 1979. *Wakamatha tasselli* gen. et sp. nov., a fossil dasyurid (Marsupialia) from South Australia convergent on modern Sminthopsis. *Memoirs of the Queensland Museum*, **19**, 309–317.

Archer, M. & **Wade, M.** 1976. Results of the Ray E. Lemley expeditions, part 1: The Allingham Formation and a new Pliocene vertebrate fauna from northern Queensland. *Memoirs of the Queensland Museum*, **17**, 54–58.

Archer, M., **Godthelp, H.**, **Hand, S. J.** & **Megirian, D.** 1989. Fossil mammals of Riversleigh, northwestern Queensland: preliminary overview of biostratigraphy, correlation and environmental change. *Australian Zoologist*, **25**, 29–65.

Archer, M., **Hand, S.** & **Godhelp, H.** 1991. *Riversleigh – The story of animals in the ancient rainforest of inland Australia*. Reed Books, Balgowlah.

Archer, M., **Hand, S. J.**, **Godthelp, H.** & **Creaser, P.** 1997. Correlation of the Cainozoic sediments of the Riversleigh World Heritage Fossil Property, Queensland, Australia. Pp. 131–152 in J.-P. Aguilar, S. Legendre & J. Michaux (eds) *Actes du Congres BiocroM'97*. Memoirs et Traveaux Ecole Pratique des Hautes Etudes, Institut de Montpellier, Montpellier.

Archer, M., **Arena, D. A.**, **Bassarova, M.**, **Beck, R. M. D.**, **Black, K.**, **Boles, W. E.**, **Brewer, P.**, **Cooke, B. N.**, **Crosby, K.**, **Gillespie, A.**, **Godthelp, H.**, **Hand, S. J.**, **Kear, B. P.**, **Louys, J.**, **Morrell, A.**, **Muirhead, J.**, **Roberts, K. K.**, **Scanlon, J. D.**, **Travouillon, K. J.** & **Wroe, S.** 2006. Current status of species-level representation in faunas from selected fossil localities in the Riversleigh World Heritage Area, northwestern Queensland. *Alcheringa Special Issue*, **1**, 1–17.

Arena, D. A. 2004. *The geological history and development of the terrain at the Riversleigh World Heritage Area during the middle Tertiary*. Unpublished PhD thesis, University of New South Wales, 275 pp.

Beck, R. M. D., **Archer, M.**, **Godthelp, H.**, **Mackness, B. S.**, **Hand, S. J.** & **Muirhead, J.** 2008a. A bizarre new family of Marsupialia (Incertae sedis) from the Early Pliocene of northeastern Australia: implications for the phylogeny of bunodont marsupials. *Journal of Paleontology*, **82**, 749–762.

Beck, R. M. D., **Godhelp, H.**, **Weisbecker, V.**, **Archer, M.** & **Hand, S. J.** 2008b. Australia's oldest marsupial fossil and their biogeographical implications. *PloS ONE*, **3**(3), e1858.

Bininda-Emonds, O. R. P., **Beck, R. M. D.** & **Purvis, A.** 2005. Getting to the roots of matrix representation. *Systematic Biology*, **54**, 668–672.

Black, K. H., **Archer, M.**, **Hand, S. J.** & **Godthelp, H.** (2012). Revision in the marsupial diprotodontid genus *Neohelos:* systematics and biostratigraphy. *Acta Palaeontologica Polonica*, http://dx.doi.org/10.4202/app.2012.0001.

Breen, J. G. 1985. *Wanyi Dialect*. School of Australian Linguistics, Darwin Community College, Darwin, 56 pp.

Bremer, K. 1988. The limits of amino acid sequence data in angiosperm phylogenetic reconstruction. *Evolution*, **42**, 795–803.

Campbell, C. R. 1976. *Tertiary Dasyurida and Peramelidae (Marsupialia) from the Tirari Desert, South Australia*. PhD thesis, University of California, Berkeley, 220 pp.

Case, J. A. 2001. Turnover of bandicoots in the Oligo-Miocene of South Australia. *Journal of Vertebrate Paleontology*, **21**(3), 39A.

Cobbett, A., **Wilkinson, M.** & **Wills, M.** 2007. Fossils impact as hard as living taxa in parsimony analyses of morphology. *Systematic Biology*, **56**, 753–766.

Cuvier, G. 1817. *Le règne animal distribué d'après son organisation, pour servir de base à l'histoire naturelle des animaux et d'introduction à l'anatomie comparée. Avec figures, dessinées d'après nature. Tome II, contenant les reptiles, les poissons, les mollusques et les annélides*. Deterville, Paris, 532 pp.

Dornburg, A, **Brandley M. C**, **McGowen M. R.** & **Near T. J.** 2012. Relaxed clocks and inferences of heterogeneous patterns of nucleotide substitution and divergence time estimates across whales and dolphins (Mammalia:Cetacea). *Molecular Biology and Evolution*, **29**, 721–736. doi: 10.1093/molbev/msr228.

Erixon, P., **Svennblad, B.**, **Britton, T.** & **Oxelman, B.** 2003. Reliability of Bayesian posterior probabilities and bootstrap frequencies in phylogenetics. *Systematic Biology*, **52**, 665–673.

Evans, H. E. 1993. The skull. Pp.128–166 in H. E, Evans (ed.) *Miller's anatomy of the dog.* 3rd edition. W. B. Saunders Company, Philadelphia.

Filan, S. L. 1990. Myology of the head and neck of the bandicoot (Marsupialia Peramelemorphia). *Australian Journal of Zoology*, **38**, 617–634.

Gurovich, Y. & **Beck, R. M. D.** 2009. The phylogenetic affinities of the enigmatic mammalian clade Gondwanatheria. *Journal of Mammalian Evolution*, **16**, 25–49.

Helgen, K. M. & **Flannery, T. F.** 2004. A new species of bandicoot, *Microperoryctes aplini*, from western New Guinea. *Journal of Zoology (London)*, **264**, 117–124.

Hershkovitz, P. 1982. The staggered marsupial lower third incisor (I3). *Geobios,* Memoir Special **6**, 191–200.

Hershkovitz, P. 1995. The staggered marsupial third lower incisor: hallmark of cohort Didelphimorphia, and description of a new genus and species with staggered i3 from the Albian (Lower Cretaceous) of Texas. *Bonner Zoologische Beiträge*, **45**, 153–169.

Hocknull, S. A. 2005. Ecological succession during the late Cainozoic of central eastern Queensland: Extinction of a diverse rainforest community. *Memoirs of the Queensland Museum*, **51**(1), 39–122.

Illiger, J. K. W. 1811. *Prodromus Systematis Mammalium et Avium*: *Additis terminis zoographicis utriusque classis, eorumque versione germanica*, C. Salfeld, Berlin, xviii + 301 pp.

Kirsch, J. A. W. 1968. Prodromus of the comparative serology of Marsupialia. *Nature*, **217**, 418–420.

Kitazoe, Y., **Kishino, H.**, **Waddell, P. J.**, **Nakjima, N.**, **Okabayashi, T.**, **Watabe, T.** & **Okuhara, Y.** 2007. Robust time estimation reconciles views of the antiquity of placental mammals. *PLoS ONE*, **2**, e384.

Ladevèze, S. 2004. Metatherian petrosals from the Late Paleocene of Itaborai (Brazil), and their phylogenetic implications. *Journal of Vertebrate Palaeontology*, **24**, 202–213.

Lewis, P. O. 2001. A likelihood approach to inferring phylogeny from discrete morphological characters. *Systematic Biology*, **50**, 913–925.

Luckett, W. P. 1993. An ontogenetic assessment of dental homologies in therian mammals. Pp. 182–204 in F. S. Szalay, M. J. Novacek & M. C. McKenna (eds) *Mammal phylogeny: mesozoic differentiation, multituberculates, monotremes, early eutherians and marsupials*. Springer-Verlag, New York.

Mackness, B. S., **Wroe, S.**, **Muirhead, J.**, **Wilkinson, C.** & **Wilkinson, D.** 2000. First fossil bandicoot from the Pliocene Chinchilla Local Fauna. *Australian Mammalogy*, **22**, 133–136.

Macphail, M. K. 1996. A habitat for the enigmatic *Wynyardia bassiana* Spencer, 1901 Australia's first described Tertiary land mammal? *Alcheringa: An Australas J Palaeontol*, **20**, 227–243.

Megirian, D., **Prideaux, G. J.**, **Murray, P. F.** & **Smith, N.** 2010. An Australian land mammal age biochronological scheme. *Paleobiology*, **36**, 658–671.

Meredith, R. W., **Westerman, M.** & **Springer, M. S.** 2008. A timescale and phylogeny for "Bandicoots" (Peramelemorphia: Marsupialia) based on sequences for five nuclear genes. *Molecular Phylogenetics and Evolution*, **47**, 1–20.

Metzger, C. A. & **Retallack, G. J.** 2010, Middle Miocene climate change in the Australian outback. *Australian Journal of Earth Sciences*, **57**, 871–885.

Muirhead, J. 1994. *Systematics, evolution and palaeobiology of recent and fossil bandicoots (Peramelemorphia, Marsupialia)*. PhD thesis, University of New South Wales, Sydney, 463 pp.

Muirhead, J. 1999. Bandicoot diversity and evolution (Peramelemorphia, Marsupialia): the fossil evidence. *Australian Mammalalogy*, **21**, 11–13.

Muirhead, J. 2000. Yaraloidea (Marsupialia, Peramelemorphia), a new superfamily of marsupial and a description and analysis of the cranium of the Miocene *Yarala burchfieldi*. *Journal of Paleontology*, **74**, 512–523.

Muirhead, J. & **Filan, S. L.** 1995. *Yarala burchfieldi*, a plesiomorphic bandicoot (Marsupialia, Peramelemorphia) from Oligo-Miocene deposits of Riversleigh, northwestern Queensland. *Journal of Paleontology*, **69**, 127–134.

Muirhead, J. & **Godthelp, H. J.** 1996. Fossil bandicoots of Chillagoe (northeastern Queensland) and the first known specimens of the pig-footed bandicoot *Chaeropus* Ogilby, 1838 from Queensland. *Australian Mammalogy*, **19**, 73–76.

Muirhead, J., **Dawson, L.** & **Archer, M.** 1997. *Perameles bowensis*, a new species of *Perameles* (Peramelomorphia, Marsupialia) from Pliocene faunas of Bow and Wellington caves, New South Wales. *Proceedings of the Linnean Society of New South Wales*, **17**, 163–174.

Muizon, C. de 1998. *Mayulestes ferox*, a borhyaenoid (Metatheria, Mammalia) from the early Palaeocene of Bolivia. phylogenetic and paleobiologic implications. *Geodiversitas*, **20**(1), 19–142.

Myers, T. J. 2001. Prediction of marsupial body mass. *Australian Journal of Zoology*, **49**, 99–118.

Nylander, J. A., **Ronquist, A. F.**, **Huelsenbeck, J. P.** & **Nieves- Aldrey, J. L.** 2004. Bayesian phylogenetic analysis of combined data. *Systematic Biology*, **53**, 47–67.

Pledge, N. S. 1987. *Muramura williamsi*, a new genus and species of ?wynyardiid (Marsupialia: Vombatoidea) from the middle Miocene Etadunna Formation of South Australia. Pp. 393–400 in M. Archer (ed.) *Possums and opossums: studies in evolution*. Surrey Beatty & Sons, and the Royal Zoological Society of New South Wales, Sydney.

Pledge, N. S. 2003. A new species of Muramura Pledge (Wynyardiidae: Marsupialia) from the Middle Tertiary of the Callabonna Basin, northeastern South Australia. *Bulletin of the American Museum of Natural History*, **279**, 541–555.

Price, G. J. 2002. *Perameles sobbei*, sp. nov. (Marsupialia, Peramelidae), a Pleistocene bandicoot from the Darling Downs, south-eastern Queensland. *Memoirs of the Queensland Museum*, **48**, 193–197.

Price, G. J. 2005. Fossil bandicoots (Marsupialia, Peramelidae) and environmental change during the Pleistocene on the Darling Downs, southeastern Queensland, Australia. *Journal of Systematic Palaeontology*, **4**, 347–356.

Rich, T. H, **Archer, M.**, **Hand, S. J.**, **Godthelp, H.**, **Muirhead, J.**, **Pledge, N. S.**, **Flannery, T. F.**, **Woodburne, M. O.**, **Case, J. A.**, **Teford, R. H.**, **Turnbull, W. D.**, **Lundelius, E. L. jr.**, **Rich, L. S. V.**, **Whitelaw, M. J.**, **Kemp, A.** & **Rich, P. V.** 1991. Australian Mesozoic and Tertiary terrestrial mammal localities, Appendix 1. Pp. 1005–1058 in P. Vickers-Rich, J. M. Monaghan, R. F. Baird & T. H. Rich (eds) *Vertebrate Palaeontology of Australia*. Pioneer Design Studio & Monash University Publications Commiitee, Melbourne.

Ronquist, F. & **Huelsenbeck, J. P.** 2003. MrBayes3: Bayesian phylogenetic inference under mixed models. *Bioinformatics*, **19**, 1572–1574.

Schwartz, L. R. S. 2006. A new species of bandicoot from the Oligocene of northern Australia and implications of bandicoots for correlating Australian Tertiary mammal faunas. *Palaeontology*, **49**, 991–998.

Simpson, G., **Roe, A.** & **Lewontin, R.** 1960. *Quantitative Zoology*. Harcourt Brace, New York.

Stirton, R. A. 1955. Late Tertiary marsupials from South Australia. *Records of the South Australian Museum*, **11**, 247–267.

Strahan, R. 1995. *Mammals of Australia*. Smithsonian Institution Press, Washington DC.

Szalay, F. S. 1982 A new appraisal of marsupial phylogeny and classification. Pp. 621–640 in M. Archer (ed.) *Carnivorous Marsupials*. Royal Zoological Society of New South Wales, Sydney.

Travouillon, K. J., **Archer, M.**, **Hand, S. J.** & **Godthelp, H.** 2006. Multivariate analyses of Cenozoic mammalian faunas from Riversleigh, north-western Queensland. *Alcheringa*, Special Issue **1**, 323–349.

Travouillon, K. J., **Legendre, L.**, **Archer, M.** & **Hand, S. J.** 2009. Palaeoecological analyses of Riversleigh's Oligo-Miocene sites: implications for Oligo-Miocene climate change in Australia. *Palaeogeography, Palaeoclimatology, Palaeoecology*, **276**, 24–37.

Travouillon, K. J., **Gurovich, Y.**, **Beck, R. M. D.** & **Muirhead, J.** 2010. An exceptionally well-preserved short-snouted bandicoot (Marsupialia; Peramelemorphia) from Riversleigh's Oligo-Miocene deposits, northwestern Queensland, Australia. *Journal of Vertebrate Paleontology*, **30**, 1528–1546.

Travouillon, K. J., **Escarguel, G.**, **Legendre, S.**, **Archer, M.** & **Hand, S. J.** 2011. The use of MSR (Minimum Sample Richness) for sample assemblage comparisons. *Paleobiology*, **37**, 696–709.

Turnbull, W. D., **Lundelius, E. L.** & **Archer, M.** 2003. Dasyurids, perameloids, phalangeroids and vomabatoids from the early Pliocene Hamilton fauna, Victoria, Australia. *Bulletin of the American Museum of Natural History*, **279**, 513–540.

Van Dyck, S. 2002. Morphology-based revision of *Murexia* and *Antechinus* (Marsupialia: Dasyuridae). *Memoirs of the Queensland Museum*, **48**(1), 239–330.

Voss, R. S. & **Jansa, S. A.** 2003. Phylogenetic studies on didelphid marsupials II. Nonmolecular data and new IRBP sequences: separate and combined analyses of didelphine relationships with denser taxon sampling. *Bulletin of the American Museum of Natural History*, **276**, 1–82.

Voss, R. S. & **Jansa, S. A.** 2009. Phylogenetic relationships and classification of didelphid marsupials, an extant radiation of New World metatherian mammals. *Bulletin of the American Museum of Natural History*, **322**, 1–177.

Waddell, P. J. 2008. Fit of fossils and mammalian molecular trees: dating inconsistencies revisited, 1–18. *arXiv* 0812.5114.

Westerman, M., **Springer, M. S.** & **Krajewski, C.** 2001. Molecular relationships of the New Guinean bandicoot genera *Microperoryctes* and *Echymipera* (Marsupialia: Peramelina). *Journal of Mammalian Evolution*, **8**, 93–105.

Westerman, M., **Kear, B. P.**, **Aplin, K.**, **Meredith, R. W.**, **Emerling, C.** & **Springer, M. S.** 2012. Phylogenetic relationships of living and recently extinct bandicoots based on nuclear and mitochondrial DNA sequences. *Molecular Phylogenetics and Evolution*, **62**, 97–108.

Wible, J. R. 2003. On the cranial osteology of the short-tailed opposum *Monodelphis brevicaudata* (Didelphidae, Marsupialia). *Annals of Carnegie Museum*, **72**, 137–202.

Wible, J. R. 2008. On the cranial osteology of the Hispaniolan solenodon, *Solenodon paradoxus* Brandt, 1833 (Mammalia, Lipotyphla, Solenodontidae). *Annals of Carnegie Museum*, **77**, 321–402.

Wilson, D. E & **Reeder, D. A.** 2005. *Mammal Species of the World: A Taxonomic and Geographic Reference.* 3rd edition. Johns Hopkins University Press, Baltimore, 2142 pp.

Woodburne, M. O., **Macfadden, B. J.**, **Case, J. A.**, **Springer, M. S.**, **Pledge, N.**, **Power, J. D.**, **Woodburne, J.** & **Springer, K. B.** 1993. Land mammal biostratigraphy and magnetostratigraphy of the Etadunna Formation (late Oligocene) of South Australia. *Journal of Vertebrate Paleontology*, **13**, 483–515.

Worthy, T. H. 2009. Descriptions and phylogenetic relationships of two new genera and four new species of Oligo-Miocene waterfowl (Aves: Anatidae) from Australia. *Zoological Journal of the Linnean Society*, **156**, 411–454.

Worthy, T. H., **Tennyson, A. J. D.**, **Archer, M.**, **Musser, A. M.** & **Hand, S. J.** 2006. Miocene mammal reveals a Mesozoic ghost lineage on insular New Zealand, southwest Pacific. *Proceedings of the National Academy of Sciences*, **103**, 19419–19423.

Wroe, S. & **Milne, N.** 2007. Convergence and remarkably consistent constraint in the evolution of carnivore skull shape. *Evolution*, **61**, 1251–1260.